Advanced methods for analysis of mixed gas diffusion in polymeric membranes

Advanced methods for analysis of mixed gas diffusion in polymeric membranes

Marcello Monteleone,[a] Alessio Fuoco,[a,*] Elisa Esposito,[a] Ian Rose,[b] Jie Chen,[b] Bibiana Comesaña-Gándara,[b] C. Grazia Bezzu,[c] Mariolino Carta,[d] Neil B. McKeown,[b] Maxim G. Shalygin,[e] Vladimir V. Teplyakov,[e] Johannes Carolus Jansen[a,*]

[a] Institute on Membrane Technology, National Research Council of Italy (CNR-ITM), via P. Bucci 17/C, Rende (CS), 87036, Italy

[b] *EaStCHEM, School of Chemistry, University of Edinburgh, Joseph Black Building, David Brewster Road, Edinburgh, Scotland EH9 3FJ, UK*

[c] *School of Chemistry, Cardiff University, Cardiff CF10 3AT, U.K.*

[d] *Department of Chemistry, College of Science, Swansea University, Swansea, SA2 8PP, UK.*

[e] *A. V. Topchiev Institute of Petrochemical Synthesis, Russian Academy of Sciences (TIPS RAS), 119991, Leninsky Prospect 29, Moscow, Russia.*

Corresponding author: alessio.fuoco@cnr.it (A.F.); johannescarolus.jansen@cnr.it (J.C.J.)

ABSTRACT

The rapid advancement of membrane gas separation processes has spurred the development of new and more efficient membrane materials, including polymers of intrinsic microporosity. The full exploitation of such materials requires thorough understanding of their transport properties, which in turn necessitates the use of powerful and reliable characterization methods. Most methods focus on the permeability, diffusivity and solubility of single gases or only the permeability of mixed gases, while studies reporting the diffusion and solubility of gas mixtures are extremely rare. In this paper we report the use of a mass-spectrometric residual gas analyser to follow the transient phase of mixed gas transport through a benzotriptycene-based ultrapermeable polymer of intrinsic microporosity (PIM-DTFM-BTrip) and a polydimethylsiloxane (PDMS) membrane for comparison, via the continuous online analysis of the permeate. Computational analysis of the entire permeation curve allows the calculation of the mixed gas diffusion coefficients for all individual gases present in the mixture and the identification of non-Fickian diffusion or other anomalous behaviour. The mixed gas transport parameters were analysed by three different approaches (integral, differential and pulse signal), and compared with the results of the 'classical' time lag method for single gases. PDMS shows very similar results in all cases, while the transport in the PIM gives different results depending on the specific method and instrument used. This comparative study provides deep insight into the strengths and limitations of the different instruments and data elaboration methods to characterize the transport in rubbery and high free volume glassy membranes with fundamentally different properties and will be of help in the development of novel membrane materials.

Keywords

Gas separation membrane, solution-diffusion model, mixed gas diffusion, time lag, transport properties, mathematics of diffusion.

1. Introduction

In a variety of industrial gas separation processes, such as oxygen enrichment or pure nitrogen production from air (O_2/N_2) [1], hydrogen separation from ammonia tail gas (H_2/N_2) [2,3], natural gas sweetening (CO_2/CH_4) [4,5], membrane-based gas separation processes are a consolidated technology [6,7]. It is emerging or under study for other separations, such as biogas upgrading (CO_2/CH_4) [8,9] or carbon capture from flue gas (CO_2/N_2) [10–12]. The successful introduction of new applications requires the best possible materials and process configuration for that specific separation [13], and this, in turn, requires precise knowledge of their transport properties.

1.1. Gas transport in dense membranes

It is well-known that the transport of gases in dense membranes takes place according to the so-called Solution-Diffusion mechanism [14,15], in which the gas is first absorbed in the membrane at the high-pressure side, to then diffuse across the membrane in the direction of decreasing concentration gradient, and finally desorb at the downstream side. In the simplest and most commonly used description, the gas solubility is constant and the equilibrium concentration follows Henry's law:

$$c = p \times S \qquad \text{Eq. 1}$$

where c is the gas concentration in the membrane in equilibrium with the feed gas, p is the feed pressure (or partial pressure of the gas) and S is the gas solubility coefficient. The gas diffusion coefficient, D, follows Fick's first and second law, defining the diffusion flow rate, J, in one dimension as:

$$J = -D \times A\frac{dc}{dx} \qquad \text{Eq. 2}$$

$$\frac{dc}{dt} = D \times \frac{d^2c}{dx^2} \qquad \text{Eq. 3}$$

where dc/dx is the concentration gradient across the membrane, dc/dt its change in time, and A is the area of the membrane. Eq. 2 and Eq. 3 are completely true only when D is not a function of the concentration in the membrane, and the simplest theories used to describe the transport and to calculate the permeability, solubility and diffusion coefficients of the gases, rely on a series of assumptions such as a constant, concentration- and time-independent D and S. In this model and with these assumptions, the permeability, P, can be calculated as:

$$P = D \times S \qquad \text{Eq. 4}$$

Most studies on the transport properties of new membranes rely on conceptually simple measurements, often only concerning single gases that give, at best, an approximation of the membrane performance in their final application. In practice, for many materials the situation is much more complex, and *S* and *D* are either not constant with time or pressure or they depend on the presence of other gas species in the mixture. Therefore, it is useful to analyse the behaviour of a membrane under different conditions and assess how much it differs from ideality. Such studies require a careful experimental investigation of the process with the most suitable methods. With that in mind, the present manuscript will discuss the advantages and limitations of the different methods for the analysis of the gas transport properties of membranes, discussing several advanced measurement techniques and data elaboration methods, with the aim of providing a deeper insight into the transport properties of novel membrane materials. We will describe the transport in two very different polymers: the rubbery polydimethylsiloxane (PDMS), and the glassy ultrapermeable polymer of intrinsic microporosity PIM-DTFM-BTrip [16] (Figure 1).

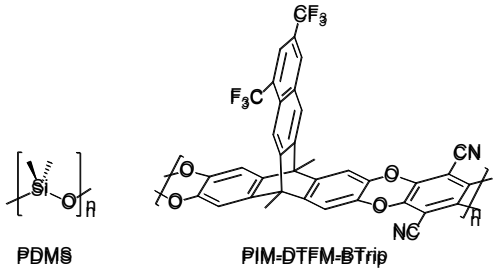

Figure 1. Polymers used in the present work.

PDMS is a benchmark polymer for gas separation applications, and at room temperature, it is far above its crystalline melting point, so it is in its amorphous rubbery thermodynamic equilibrium state. Instead, PIM-DTFM-BTrip is an amorphous glassy polymer in a thermodynamic non-equilibrium state, far below its glass transition temperature, which is usually above the degradation temperature for PIMs [17]. PIM-DTFM-BTrip contributed to the definition of the latest CO_2/CH_4 and CO_2/N_2 upper bounds [16] due its particular 2D chain structure [18] and high rigidity [19]. The latter is common for PIMs [20] and, in combination with the contorted backbone structure, prevents the efficient packing of the polymer chains in the solid state, providing a large fractional free volume [21,22], which typically results in high permeability and high selectivity. This combination makes PIMs responsible for all the main shifts in the Robeson Upper bounds since 2008 [16,23–25]. The fluorinated groups in PIM-DTFM-BTrip are likely to decrease the cohesive forces in the polymer matrix, reducing its tendency to undergo physical aging, a feature that makes glassy perfluoropolymers rather unique, because they tend to age less rapidly [26] compared to other high free volume polymers such as poly(trimethylsilylpropyne) PTMSP [27]. At the same time, their high hydrophobicity is expected to make the permeability less influenced by the humidity in the gas stream [28] and its fluorinated nature provides unique

sorption properties [29]. PIMs are furthermore known to be sensitive to pressure and to mixed gas composition [24], the feature that makes them most interesting for this comparative study.

1.2. Methods for the analysis of transport parameters

The most straightforward methods employed to analyse the transport properties in membranes, measure directly the gas permeation rate in either a dead-end cell, in the case of pure gases or vapours, or in a cross-flow cell for mixtures [30]. The permeate flow rate can be measured directly, with a bubble flow meter or more sophisticated electronic flow meters, or indirectly, via the concentration in a sweeping or carrier gas with known flow rate [31]. In a fixed volume setup, it is calculated from the pressure increase rate of the permeate volume. The gas solubility can be determined directly via gravimetric or volumetric sorption measurements, even in complex systems [32], and the diffusion coefficient, i.e. the transport diffusivity of permeating gases, can be assessed under transient conditions from either sorption kinetics [33] or permeation kinetics measurements, the latter typically via the so-called time lag method. Other methods include more complex analysis, such as NMR spectroscopy [34,35] or molecular modelling approaches [36,37]. While well-calibrated instruments should be able to provide the same results, this is often not the case because of the materials properties and the measurement principle used or because of the operational conditions [38,39].

The time lag method for the analysis of the diffusion coefficient in polymer films was first reported about a century ago by Daynes [40]. Since then, it became by far the most commonly used technique for the analysis of gas transport parameters in polymers and in porous materials [41]. Its use has been extended to the quantification of hydrogen diffusion in metals [42] or even to salt diffusion in liquid phase membranes [43] with the latter using not only the downstream concentration but also the upstream concentration [44]. In its simplest form, the method consists in the measurement of the total amount of gas in the permeate, usually determined as the pressure in a fixed permeate volume. The method showed some limitations, related to the effect of the instrument itself on the gas transport [45–47], in combination with non-ideal properties of the materials [48]. This might require minor adjustments in the calculations, but these are usually only important in some extreme cases and they did not prevent this method becoming one of the most widely used techniques.

One of the most important limitations of the classical time lag technique is that the measurement of pressure allows the analysis of a single species only. It is much more difficult to determine the transient behaviour and to obtain information on diffusion and solubility of gas mixtures, because the most commonly used gas chromatographic analysis of the permeate composition is too slow to follow the transient phase of permeation. Thermal conductivity detectors can be used to follow changes in the permeate (sweep gas + permeate) continuously [31], but they are unable to analyse the composition of complex mixtures, for which a combination with for instance gas chromatography (GC) is needed. Several methods have been reported, based on sorption measurements [49–52], on permeation measurements with selective condensation of the least volatile component [53,54], on computer simulations [55,56] or on alternative techniques such as NMR spectroscopy [35]. Many of these suffer from complex experimental procedures or data elaboration methods. Various studies have proposed online mass spectrometry to measure the permeation transient in pervaporation [57,58] or gas permeation [59–61]. This requires a more sophisticated instrumentation (mass spectrometer),

but it facilitates the measurement procedure. Inspired by this earlier work, we designed a gas permeability setup with fast online analysis of the permeate composition in a standard cross-flow cell via mass spectrometry [62], and we further optimized this method for the determination of the mixed gas diffusion coefficients [63,64], that is also suitable for highly permeable polymeric membranes with a fast transient, unlike much slower GC analysis. The method determines the time lag by the tangent-method in a plot of the cumulative permeate volume versus time, measured via online analysis of the gas composition in the permeate by mass spectroscopy, followed by integration of the concentration over time to yield the total amount of permeate. The time lag must be corrected for the instrumental delay, namely the time lag determined from the response of the system when exposing an aluminium disk with pinhole to the gas, or when extrapolating the time lag of membranes with different thicknesses to zero thickness. We assumed that the instrumental time lag corresponded to average residence time of the gas in the system without membrane. The response of the system was found to be slightly slower at higher pressure, because of the need to pressurize the feed line with the gas [64]. For a somewhat analogous situation, where the Knudsen diffusion of the gas from the membrane to the analyser causes an additional delay, Kruczek *et al.* showed that the correction factor should not be equal to the time lag due to the Knudsen diffusion, but slightly smaller [45]. For the flow of a gas pulse in a cylindrical tube, Evans and Kenney discussed that the average residence time of a species flowing in a laminar flow corresponds to the peak maximum at a distance from the injection point [65], analogous to what Tailor described for liquid flow [66]. This suggests that the time lag of the membrane-less system is indeed not the best correction for the instrumental delay, as we have assumed previously [63], because it slightly deviates from the average residence time. For diffusion in dense membranes, Beckmann *et al.* have discussed the comparison between the classical pressure increase curve with its derivative, corresponding to the typical permeate concentration curve or flow rate curve after a step change in a cross-flow cell, and with its second derivative, corresponding to the signal after a pulse change in the feed concentration [67,68] (see Section 5).

Recently we have shown that we can also determine the permeation time lag directly from the measured permeate flow rate as a function of time, *i.e.* from the original signal, which is the mathematical derivative of the time lag curve [69]. The inflection point in this sigmoidal curve corresponds to the peak in the pulse signal, and the inflection point of the signal in a membrane-free test run can be used for the correction of the instrumental lag time.

In this work, that aims to develop even more versatile and powerful methods to characterize the transport properties of membrane materials for gas separation, we compared each of the above methods to measure mixed gas permeation and diffusion, via the integral or time lag curve, the derivative curve, and the pulse curve, using two fundamentally different materials. Being glassy polymers with high free volume, PIMs are known for their deviation from simple Fickian diffusion and for their pressure- and composition-dependent transport properties. PDMS will therefore be used for the method setup and for comparison as a well-defined benchmark membrane material, while PIM-DTFM-BTrip is used for validation and analysis of the sensitivity and the strengths and limits of the methods.

2. Experimental

2.1. Materials and membrane preparation

A dense PDMS membrane was prepared from a two-component resin (SYLGARD® 184, Dow Corning Midland). The prepolymer and crosslinker were mixed in the ratio 10:1 according to the instructions of the supplier, and the resin was cured at room temperature over the weekend in a Teflon Petri dish. The final membrane thickness resulted 1056 ± 23 μm, measured with a Mitutoyo model IP65 digital micrometer as an average of 10 points. The exposed area inside the footprint of the sealing ring was 13.84 cm^2 for both the pure and mixed gas permeability measurements.

An aluminium sample with a pinhole was prepared by puncturing a 50 μm thick aluminium disk (Ø 47 mm) with the extremity of a syringe needle, to leave an imperceptible pinhole that is only visible by the naked eye in backlight and that exhibits a nitrogen flow rate of 0.92 cm^3_{STP} min^{-1} at 1 bar. This is in a similar range as the CO_2 permeability of the most permeable membranes, and thus it allows the use of the same calibration data.

The PIM used in this study was PIM-DTFM-BTrip (Figure 1) and its preparation was described previously [16]. The membrane was prepared by solution casting from quinoline, solvent evaporation, and subsequent treatment with methanol to remove the residual solvent and reset the sample history. The sample was masked with aluminium adhesive tape to reduce its active area to 0.785 cm^2 and the average thickness in this area was 112 ± 6 μm. A long-term 1380 days aged sample, with well-known physical-chemical properties and ageing history [16], was used to guarantee maximum stability of the sample during the measurement campaign.

2.2. Gas permeation measurements

Pure gas (fixed volume instrument) and mixed gas (fixed pressure instrument) permeation measurements were carried out with setups already described previously [63], and the detailed description of the standard experimental procedures are reported in the supporting information. The unique feature of the mixed gas permeation setup is that the gas composition is analysed continuously by means of a mass spectrometric residual gas analyser, which allows the simultaneous determination of multiple gas species in a mixture.

The nonstandard pulse measurements, with a short exposure of the membrane to the gas or gas mixture, were carried out flushing the feed side with a dilute certified mixture, containing 3% CO_2 and 3% CH_4 in argon, instead of pure argon before the measurement. This moderately increases the baseline signal for CH_4 and CO_2 and allows a higher measurement frequency and more accurate analysis. The feed stream is then substituted by the gas of interest by setting directly its flow rate at the maximum of 500 cm^3 min^{-1} with the mass flow controller, rather than switching the six-way valve as seen in the differential method. Thus, at fixed moments, the membrane is exposed to pulses of the gas of interest for 1s, 2s, 4s, 6s, 8s and 10s at a flow rate of 500 cm^3 min^1. The use of the MFCs for the pulse control causes a slightly slower response of the system, compared to the manual switching of the six-way valve, but it can be controlled entirely by the Flowplot software. This procedure is repeated for at least three different pressures, both for the membrane samples and

for the control sample with pinhole. The raw MS signal is then elaborated by the procedure reported previously [63] to calculate the volumetric permeate flow rate at STP conditions.

2.2.1. Data elaboration

The fixed volume instrument provides the data of the permeate pressure (in mbar with 4 decimals) and the feed pressure as a function of time and these are elaborated as such [63]. The raw MS measurement signal (gas partial pressure in Torr as a function of time) is elaborated by the procedure reported by Fraga *et al.* [63], using argon as the internal standard to calculate the volumetric permeate flow rate (in STP) as a function of time as the basis for further elaborations. The background signal of the MS residual gas analyser is subtracted before calculation of the flow rates.

The experimental data are fitted with the appropriate equations described in Annex 1, namely: Eq. A1 for the permeation curves obtained in the fixed volume setup; Eq. A5 for the cumulative permeate volume obtained in the fixed pressure setup or after integration of the differential signal, as described in detail by Fraga *et al.* [63]; Eq. A10 for the sigmoidal (derivative) curve obtained after calculation of the permeate flow rate from the raw MS data; and Eq. A11 for the experimental data obtained via the pulse method. The fitting was performed using least square method and the Excel nonlinear Generalized Reduced Gradient (GRG) solver algorithm, after expansion of the Tailor series into 25 terms. The GRG algorithm finds local optimal solutions, which means that the final solution could depend on the guessed starting points, and this is generally recognized by the poor visual fit of the experimental data. For this reason, for all the fitting procedures the initial starting points in the minimization procedure of D and S were set close to the values obtained by the tangent method, and only if this did not lead to a satisfactory fit, the starting values were adjusted manually. The terms related to starting permeate pressures and instrumental leak flow rate were set to zero since they were found to be negligible for the tested membranes in these testing conditions.

3. Results and discussion

3.1. Gas transport measured by the fixed volume setup

The fixed volume setup is the instrument with the fastest response. The aluminium film with pinhole reaches steady state permeation within a second (Figure SI2) and extrapolation of the steady-state pressure increase curves yields an instrumental time lag of 0.08±0.02 s, independent of the gas type, feed pressure and permeate volume. This extremely fast response confirms that there is no significant contribution of the instrument itself to the time lag, and therefore no corrections related to the transport of the gas in the downstream side are needed [46,47]. This very short instrumental time lag is indeed negligible compared to the time lag of the same gases in the majority of thick dense polymeric membranes, with exception of extremely fast-diffusing gases such as He and H_2 in very thin membranes or in highly permeable polymers, such as PIMs. Details are given in the supplementary information.

3.1.1. *Tangent method: PDMS vs PIM-DTFM-BTrip:*

The original permeation curves of H_2, He, O_2, N_2, CH_4 and CO_2 in PDMS and PIM-DTFM-BTrip are displayed in Figure 2. The curves do not show any perceptible anomalies in both materials, and the initial pressure and the initial slope are completely negligible, excluding the presence of significant leaks in the membranes or in the system. The time lag was determined by the tangent method, fitting a straight line through the curve in the linear part from approximately 5x the value of the eventual time lag to the end of the measurement. The time lag in the PDMS film falls in the range of 25-35 s for He and H_2, and 100-150 s for the other gases, O_2, N_2, CH_4 and CO_2. The differences with the PIM are much larger and the permeation curves show immediately some qualitatively interesting features. The time lag of O_2 is much shorter than that of CO_2, due to faster diffusion, but the permeability of CO_2 is higher, and thus the final slope of CO_2 is steeper. Instead, N_2 and CH_4 have virtually the same permeability (and thus final slope), but the diffusion in CH_4 is significantly slower. The time lag of He and H_2 is much shorter than that of all other gases

The quantitative data for *P*, D and S are listed in Table 2 and Table 3 for PDMS and PIM-DTFM-BTrip, respectively. This large difference in the diffusion coefficients of the six gases in PIM-DTFM-BTrip, confirms its high size selectivity compared to PDMS, and this is due to its highly rigid glassy nature [20]. The perfectly linear pressure-increase rate in steady state and the qualitative shape of the curves give indications of evident anomalies in the transport in both materials related, for instance, to a downstream pressure accumulation for materials with strongly non-linear sorption isotherms [48], as observed previously for Amine-PIM-1 [70,71]. The enormous difference in size-selectivity between PDMS and PIM-DTFM-BTrip is shown by the very steep correlation between the diffusion coefficient and the effective diameter of the gas in the PIM (Figure SI3).

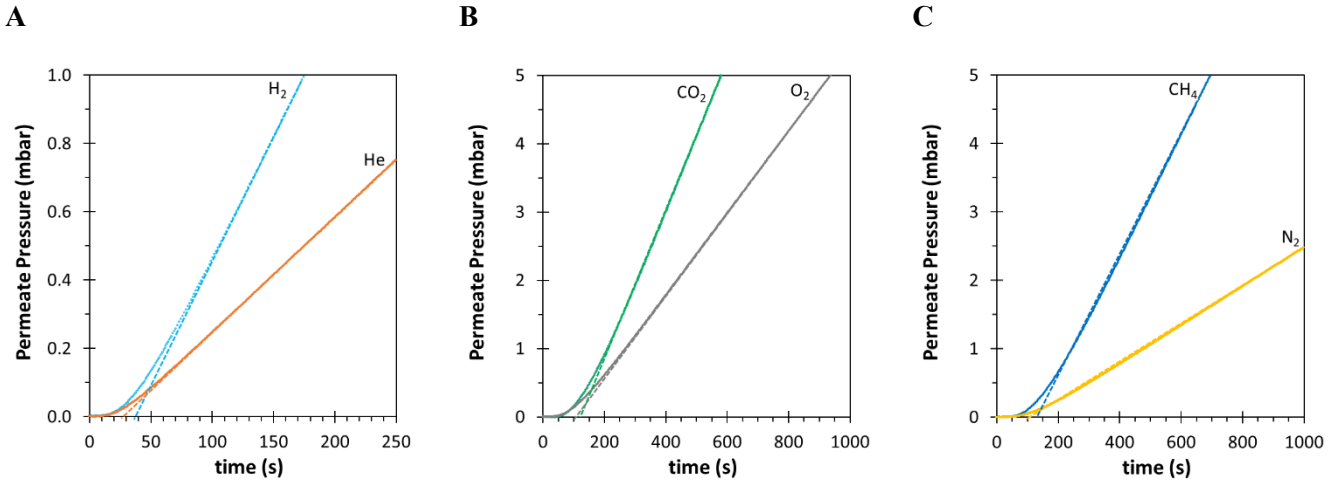

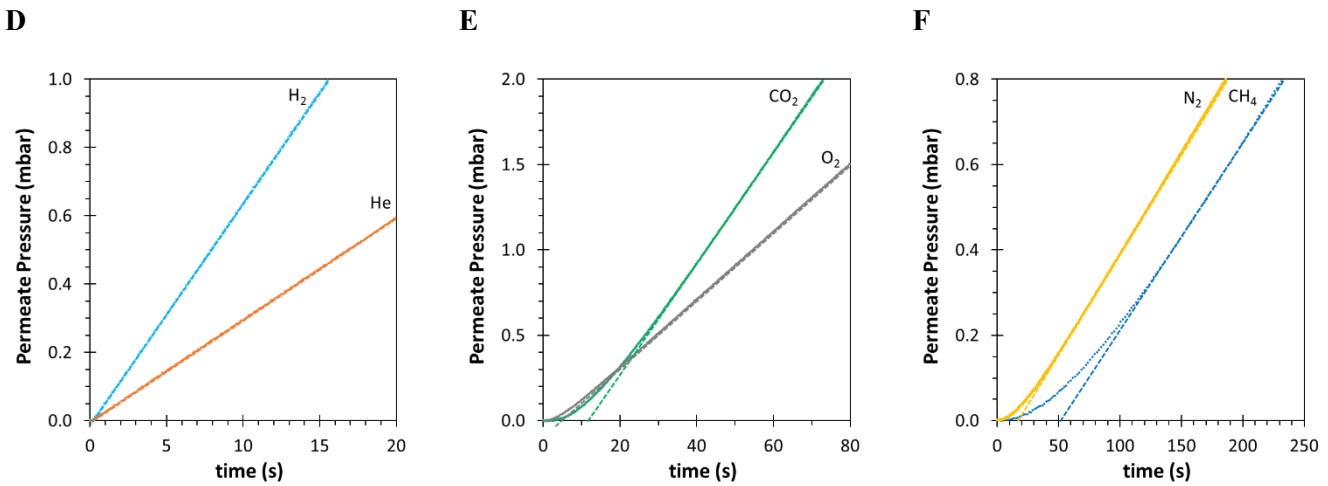

Figure 2. Time lag curves of H_2, He (A), O_2 and CO_2 (B), and N_2, CH_4 (C) in PDMS and H_2, He (D), O_2 and CO_2 (E), and N_2, CH_4 (F) in PIM-DTFM-BTrip. The intersection of the tangents (dashed lines) with the time axis show the position of the time lag.

254

255 *3.1.2. Complete curve fit*

256 The least squares fit of the permeation curve of CO_2 and CH_4 with Eq. A1 by the procedure reported in
257 section 2.2.1 is shown in Figure 3A,D. The thin lines show the extrapolated curve when fitting only part of the
258 transient zone up to the indicated time, and the calculated values of P, D, and S are plotted in Figure 3B,C,
259 E,F. Although the fitting procedure can be much more complex [72], these results highlight the advantage of
260 the fitting procedure compared to the tangent method. The PDMS curves already converge when the data are
261 fitted only until $t = 2\Theta$, *i.e.* long before pseudo-steady state is reached, whereas for the tangent method the
262 permeability and time lag are usually determined by extrapolation of the data in the interval from $t = 5\Theta$ to
263 $t = 10\Theta$. Interestingly, for the PIM-DTFM-BTrip membrane the curves and the resulting values of P converge
264 only after $t = 6\Theta$, while the values of D and S keep changing slightly until $t = 10\Theta$. This suggests anomalous
265 behaviour for the PIM, for instance due to a nonlinear sorption isotherm [48] and/or non-Fickian diffusion,
266 which are both very common in PIMs [73,74].

267

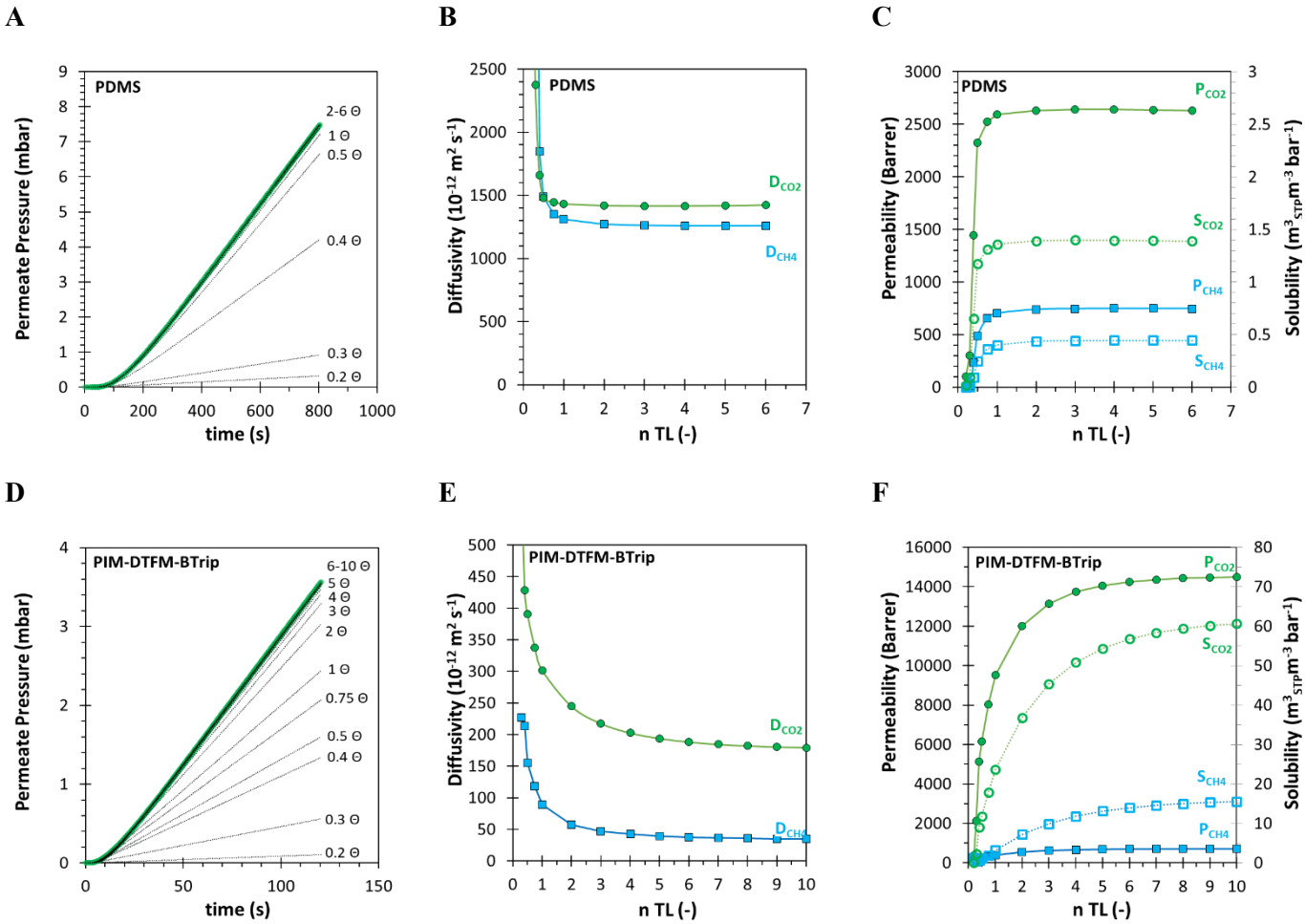

Figure 3. Least squares fit of the experimental permeation curve of pure CO_2 at a feed pressure of 1 bar in a 1056 µm PDMS membrane (A) and a 112 µm PIM-DTFM-BTrip membrane (D) according to Eq. A1. The thick green line indicates the closely spaced experimental points and the thin lines show the extrapolated curves upon a partial fit of the experimental data until the indicated time. The quantitative values of P, D, and S for CO_2 and CH_4 for the partial fit are plotted as a function of the total fit interval for PDMS until $t = 6\Theta_\infty$ (B C) and for PIM-DTFM-BTrip until $t = 10\Theta_\infty$ (E,F). Θ_∞ is the time lag obtained when the entire curve is fitted. Lines are plotted as a guide to the eye.

The residual error between the experimental data and the fit of the entire experimental curve (see Figure SI4A,C) shows very good agreement for PDMS, with less than 0.01 mbar spread for CO_2 and 0.02 mbar for CH_4, during the entire measurement time interval. Nevertheless, the weakly undulating trend in especially CH_4 is a systematic deviation shows that Eq. A1 cannot fit the data precisely. Very close examination of the permeation curve (quantitative data not shown here) reveals that this is because the slope of the curve slightly decreases after 700 s for CH_4. The situation is significantly different for the PIM. In spite of the apparently smooth determination of the time lag by the tangent method, the integral fit of permeation curve with Eq. A1 shows a marked trend in the residual errors for both CO_2 and CH_4 in PIM-DTFM-BTrip (Figure SI4B,D). Eq. A1 cannot describe the experimental permeation curve accurately and the fit underestimates the experimental

data in the initial part of the curve, because the transient is broader than expected. This is generally due to pressure-dependence of the solubility and/or the diffusion coefficient and it highlights the main advantage of the fitting procedure. It pinpoints features that the tangent method does not reveal, and thus provides much deeper insight into the transport phenomena

The pressure dependence of the transport parameters, in turn, is a result of the dual mode sorption behaviour. Not only solubility is pressure dependent, but also the diffusion of molecules in Henry's and Langmuir sites is believed to be different [33]. Especially in the case of strong interactions, the gas molecules in Langmuir sites may be partly immobilised [70,71] and the transport in PIMs or high free volume polymers in general may be even more complex than that in common glassy polymers due to possible surface diffusion [20,75]. Therefore, the traditional time lag method evaluates the transport as effective values of *P*, *D* and *S*, which may deviate significantly from the real behaviour and is a strong limitation of this method, in spite of its simplicity.

3.2. Gas transport measured by the variable volume setup

3.2.1. Differential and integral method:

The fundamental difference between the variable volume setup and the fixed-volume setup, is the additional delay due to the average residence time of the gas in the tubes, the valves, the membrane cell and the gas analyser itself, before being recorded by the analyser. This time depends on the total dead volume of the system, and on the flow rate and the pressure in the system, as shown in our previous work. We quantified this delay by two independent methods, in the first with a set of membranes of different thickness and subsequent extrapolating to zero thickness, and in the second with an aluminium disk with a pinhole that provided a negligible time lag. We corrected for this time by subtracting the instrumental time lag Θ_0 from the actual experimental time lag τ_{TL} [63].

$$\Theta_{Mem} = \frac{l^2}{6D} = \tau_{TL} - \Theta_0 \qquad \text{Eq. 5}$$

This correction, and subsequent calculation of the diffusion coefficient from the difference between the two times, assumes that the time lag of the membrane-less system corresponds to the average residence time of a gas in the system. Kruczek *et al.* proposed an analytical solution for a similar situation, where additional delay in a fixed-volume setup is caused by Knudsen diffusion in the tube between the membrane and the measurement point [45]. However, they showed that the calculation of the diffusion coefficient should not simply be based on the difference of the effective time lag and the time lag of the instrument, and the correction factor should not be equal to the time lag due to the Knudsen diffusion, but slightly smaller [45]. Indeed, in his original work on the response of a chromatographic system to a pulse injection, Tailor confirmed that the peak maximum corresponds to the average residence time of the solute in the system, which corresponds to a shorter time than the time lag [66]. Thus, the average residence time corresponds to the maximum in the curve in Figure A1C, which coincides with the inflection point in Figure A1B.

In this work, the system's response was determined by measuring the CO_2 and CH_4 flow rate through an aluminium disk with a pinhole, immediately after switching from argon purge gas to the feed gas. The resulting

sigmoidal differential signal was used as such, without integration. This signal shows a very abrupt step in the permeate concentration (Figure SI5) and to be fitted correctly with a similar equation as Eq. A10, an additional lag time, t_0, needs to be introduced. In the absence of leak flows or baseline signal, i.e. when $\left(\frac{dV_t}{dt}\right)_{0,STP} = 0$, the permeate flow rate is described by the following equation:

$$\frac{dV_{t,STP}}{dt} = A \cdot p_f \cdot S \cdot \frac{D}{l} \cdot \left(1 + 2\sum_{n=1}^{\infty}(-1)^n \, exp\left(-\frac{D \cdot n^2 \cdot \pi^2 \cdot (t - t_0)}{l^2}\right)\right) \qquad \text{Eq. 6}$$

The numerical values of the fit results are given in the supporting information (Table SI1). The data for CO_2 and CH_4 are very similar, and also the data of the pure gases and the mixtures. The average of the four measurements gives the inflection point τ_{INF} 20.1 ± 2.1 s. Using the above correction of the instrumental inflection point, we are able to evaluate the transport parameters of the PDMS membrane and the PIM-DTFM-BTrip membrane directly from the differential signal with a 35/65 Vol% CO_2/CH_4 mixture and with the pure gases at 1 bar(a) total feed pressure. The measurement was carried out as in our previous work, switching from argon purge gas to the feed gas with the 6-way valve. The normalized results are plotted in Figure 4, where each gas is normalized for its steady state flow rate for immediate comparison of the curve shape, and thus the diffusion behaviour. The permeation kinetics of CO_2 as a pure gas and as a mixture of 35 Vol% CO_2 in methane are identical in the PDMS film, and Eq. A10 fits the data perfectly, without any perceptible difference between the two fits (Figure 4A). Analogously, Eq. A10 fits the CH_4 data very well in PDMS, but in this case the mixed gas CH_4 curve slightly anticipates the pure gas curve, which means that CH_4 diffusion is slightly faster in the mixture (Figure 4B). This situation is remarkably different in the PIM, where CO_2 diffusion in the mixture is slightly slower than that of the pure gas, and CH_4 diffusion is much faster with the mixture than with the pure gas. More importantly, Eq. A10 fails to fit the CH_4 data and to a lesser extent also the CO_2 experimental data (Figure 4C,D). Thus, the fit parameters provide accurate transport parameters *P*, *D* and *S* of CO_2 and CH_4 in PDMS but they give at best a rough estimation in PIM-DTFM-BTrip, i.e. the effective averaged values under the given experimental conditions. The numerical values of the transport parameters are summarized in Table 2 and Table 3. The fundamentally different behaviour of PDMS and the PIM can be associated to the time scale needed for the polymer segment rearrangement, which is fast in PDMS and slow in the superglassy PIM, even slower with respect to glassy polycarbonates [76] where the more condensable permeant, i.e. CO_2, acts as dilating agent enhancing the diffusivity of bulkier molecules, i.e. CH_4.[77,78]

One of the reasons for the poor fit of the PIM permeation curve is the nonlinear sorption and the deviation from simple Fickian diffusion in the PIM. Therefore, the transient is very broad and it takes a relatively long time to reach steady state, as discussed above in relation to Figure 3. The second reason is that the diffusion in the PIM is so fast that the transient phase is significantly broadened by instrumental factors. This is at the same time a weakness and a strength of this method, because it makes quantitative determination of the transient phenomena (and thus the diffusion coefficient and the solubility) difficult, but its extreme sensitivity makes this method very effective for the recognition of anomalies in the transport phenomena. It must be noted that this strong deviation from the ideal behaviour is not easily detected when only the tangent

method is used, as seen in section 3.1.1, and in the majority of the studies reported in the literature. Indeed, Figure 5 shows the integral of the signals in Figure 4, which take the form of classical time lag curves because they show the total amount of permeate gas as a function of time with the difference, compared to the classical time lag measurements in a fixed volume setup, that it can simultaneously analyse different components in gas mixture. Also in this case, the fit of the curves with Eq. A5 is nearly perfect for PDMS and shows deviations for the PIM, but these deviations seem much less significant than those in Figure 4.

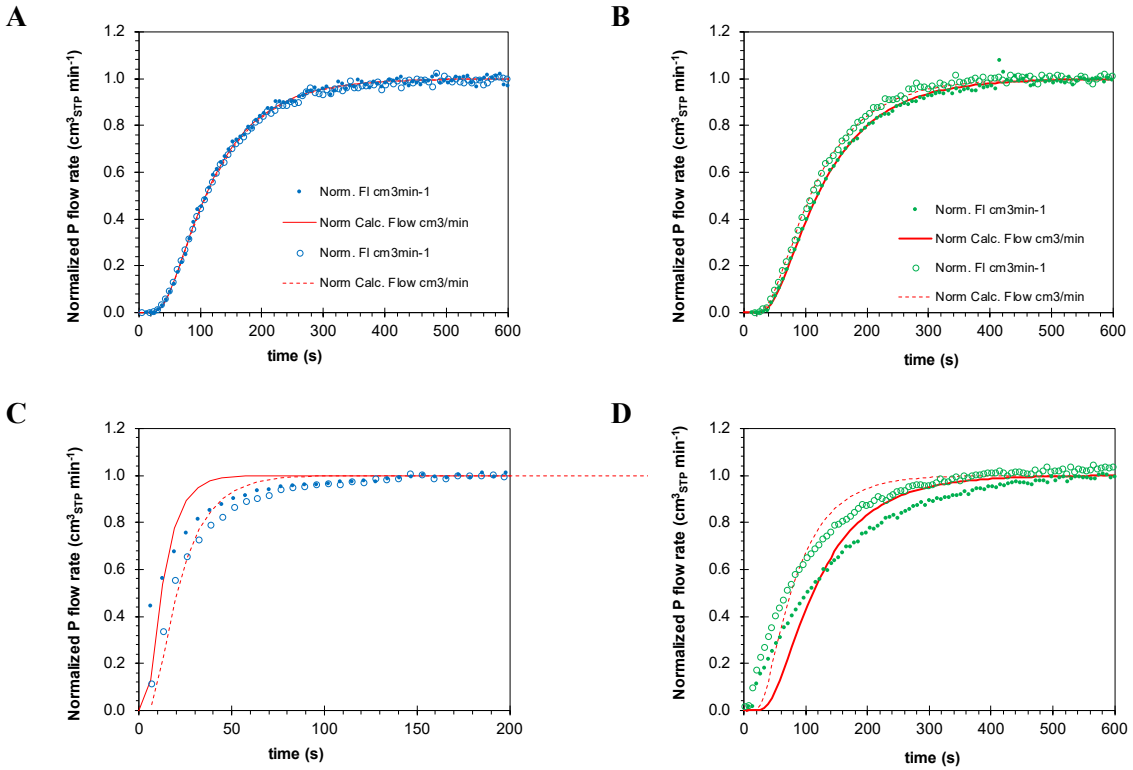

Figure 4. Comparison of the normalized pure and mixed CO_2 permeation curves by the **differential method** in (A) PDMS and (C) PIM-DTFM-BTrip, and pure and mixed CH_4 permeation curves in (B) PDMS and (D) PIM-DTFM-BTrip. Feed pressure 1 bar(a) of pure gases or of a 35/65 vol% CO_2/CH_4 mixture. Filled symbols for the pure gases and empty symbols for the mixed gases. The continuous and dashed lines represent the least squares fit of the experimental data with Eq. A10 for pure and mixed gases, respectively. Note the different time scale only for CO_2 permeation in PIM-DTFM-BTrip. The PDMS curves are horizontally shifted for 20.1 seconds to correct for the instrumental lag time, using the average time to reach the inflection point during permeation of the same gases in an aluminium disk with pinhole (Table SI1).

The integral method also allows the determination of the mixed gas diffusion coefficient, by calculation of the time lag from the tangent to the steady state volume increase curve and after subtraction of the instrumental time lag [63]. The numerical values of the transport parameters obtained by the fit of the complete curve and obtained by the tangent method are summarized in Table 2 and Table 3.

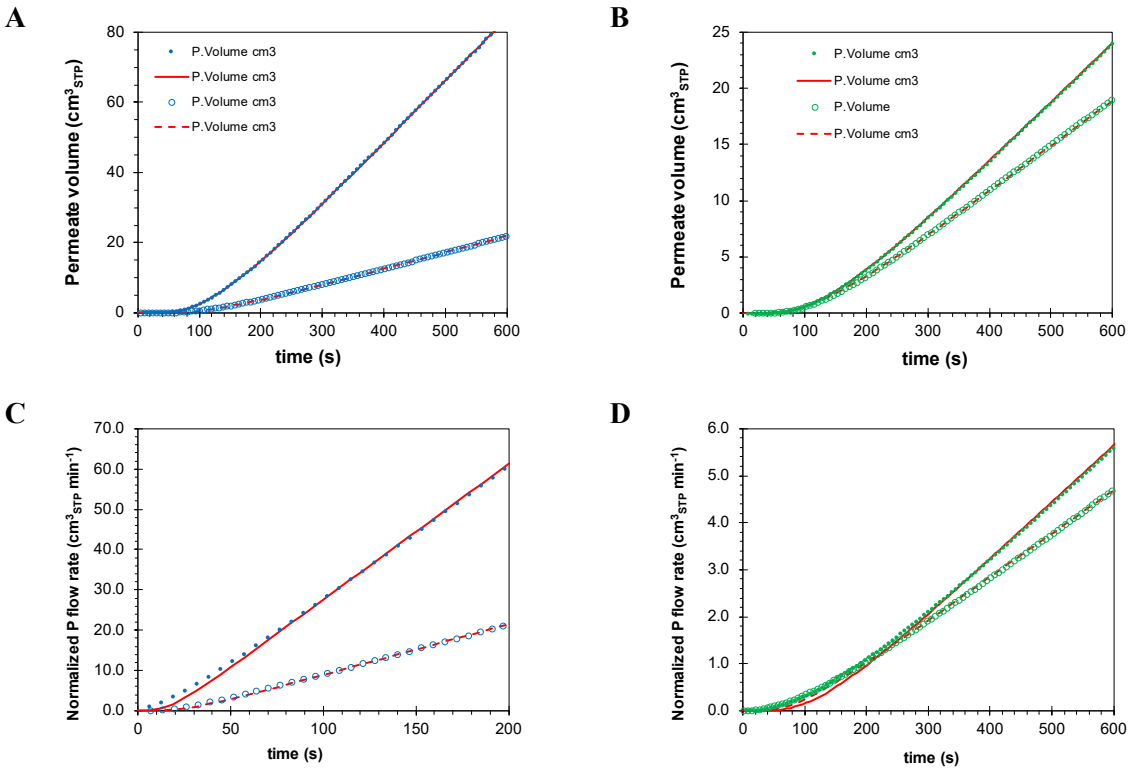

Figure 5. Comparison of the pure and mixed CO_2 permeation curves by the integral method in (A) PDMS and (C) PIM-DTFM-BTrip, and pure and mixed CH_4 permeation curves in (B) PDMS and (D) PIM-DTFM-BTrip. Feed pressure 1 bar(a) of pure gases or of a 35/65 vol% CO_2/CH_4 mixture. Filled symbols for the pure gases and empty symbols for the mixed gases. The continuous and dashed lines represent the least squares fit of the experimental data with Eq. A5 for pure and mixed gases, respectively. Note the different time scale only for CO_2 permeation in PIM-DTFM-BTrip. The PDMS curves are horizontally shifted for 20.1 seconds to correct for the instrumental lag time, using the average time to reach the inflection point during permeation of the same gases in an aluminium disk with pinhole (Table SI1).

3.2.2. *Pulse method*

3.2.2.1. Method development, instrumental delay time with pinhole

The instrumental residence time is calculated as the maximum in the signal for an aluminium disc with the pinhole after a short pulse with the gas of interest. Ideally, the pulse should be infinitely short, and thus very high to get a reasonably strong signal but, in our setup, the height is limited by the feed pressure, and very short pulses may therefore produce too weak signals. Therefore, some optimization was needed and the instrumental delay was studied with pulses of variable duration, and the experiments were carried out at different pressures. Examples of the response curves of CO_2 and CH_4 are given in Figure SI6 and Figure SI7, respectively. For a given volumetric flow rate, the size of the peak increases with pressure and with pulse

duration, because of the longer exposure and the larger amount of gas permeating through the pinhole at a higher driving force. While the onset of permeation is relatively constant, also the time of the peak maximum increases both with the feed pressure and with the pulse duration. A plot of the time of the peak maximum as a function of the pulse duration and the pressure is shown in Figure 6, showing a linear dependence of the peak time on the pressure and on the pulse duration. Indeed, it should be expected that the response of the pulse signal on changes in the feed gas stream depends on the average residence time of the gas in the system and should be directly related to the volumetric flow rate and the volume of the system. According to Tailor, the average residence time corresponds to the peak maximum [66], and thus:

$$\tau_{Max} = \tau_{Max,0} + \frac{V_{Upstream}}{\Phi_{V,F}} \qquad \text{Eq. 7}$$

Where $\tau_{Max,0}$ is the delay of the peak maximum after the pulse, due to the average residence time of the gas in the permeate side, V_{Upstream} is the volume in the upstream side and $\Phi_{\mathrm{V,F}}$ is the volumetric flow rate of the feed stream. The latter is inversely proportional to the pressure:

$$\Phi_V = \frac{\Phi_{V,STP}}{p_F} \qquad \text{Eq. 8}$$

And thus: effect of pressure on the response of the pulse in the permeate is given by:

$$\tau_{Max} = \tau_{Max,0} + \frac{p_F \times V_{Upstream}}{\Phi_{V,STP}} \qquad \text{Eq. 9}$$

Besides some scatter, the trend in the data for each pulse duration fits reasonably well with a straight line in Figure 6A and Figure 6C. The value of $\tau_{\mathrm{Max,0}}$ in Eq. 9 depends on the configuration of the gas analyser itself, and on ratio between the volume of the connections at the permeate side and the sweep (+permeate) flow rate, but these parameters were not changed in this work and, therefore, $\tau_{\mathrm{Max,0}}$ can be considered constant. Since the feed gas was changed by the mass-flow controller, and not instantaneously by switching the 6-way valve, some of the delay in the response may be due to the slow response of the MFC, causing an imperfect step in the partial pressure of the feed stream, as described by Favre et al. for the time lag method [79]. In the case of CO_2, the peak maxima range from ca. 14 s to 21 s at 2 bar and from ca. 17 s to 24 s at 6 bar. This relatively narrow range and the low standard deviations of 0.291 s for CO_2 and 0.725 s for CH_4 mean that once the conditions of pressure and pulse duration are fixed, the signal delay due to the instrumental residence time can be estimated accurately. Nevertheless, the determination of the peak maximum from the highest measurement point may cause some scatter due to the low sampling frequency of the MS signal. The fit of the entire peak would probably reduce the scatter in the calculation of the maximum, but this is much more laborious and since the standard deviation is less than 1 second, we considered this accurate enough for the present work.

The original data in Figure SI6 and Figure SI7 show that the 4 s pulse and 6 s pulse show the best compromise between a sufficiently large but not too broad peak, modest peak deformation, and a short time to reach the peak maximum. Therefore, for our further work we decided to use the 6 seconds pulse duration and the average instrumental residence time is determined from the maximum in the permeate signal of the aluminium disc with a pinhole, after exposure to a pulse of this duration with the gas of interest. Since the peak

maximum depends on the pulse time, the same pulse length should be considered for the correction if the membrane is also exposed to a pulse. Instead, if the membrane is exposed to a step-change in the feed, *i.e.* in the case of the differential signal in the previous section (Section 3.2.1), the pulse length should be extrapolated to zero to find the position of the inflection point. The latter is used for the correction of the time axis in Figure 4.

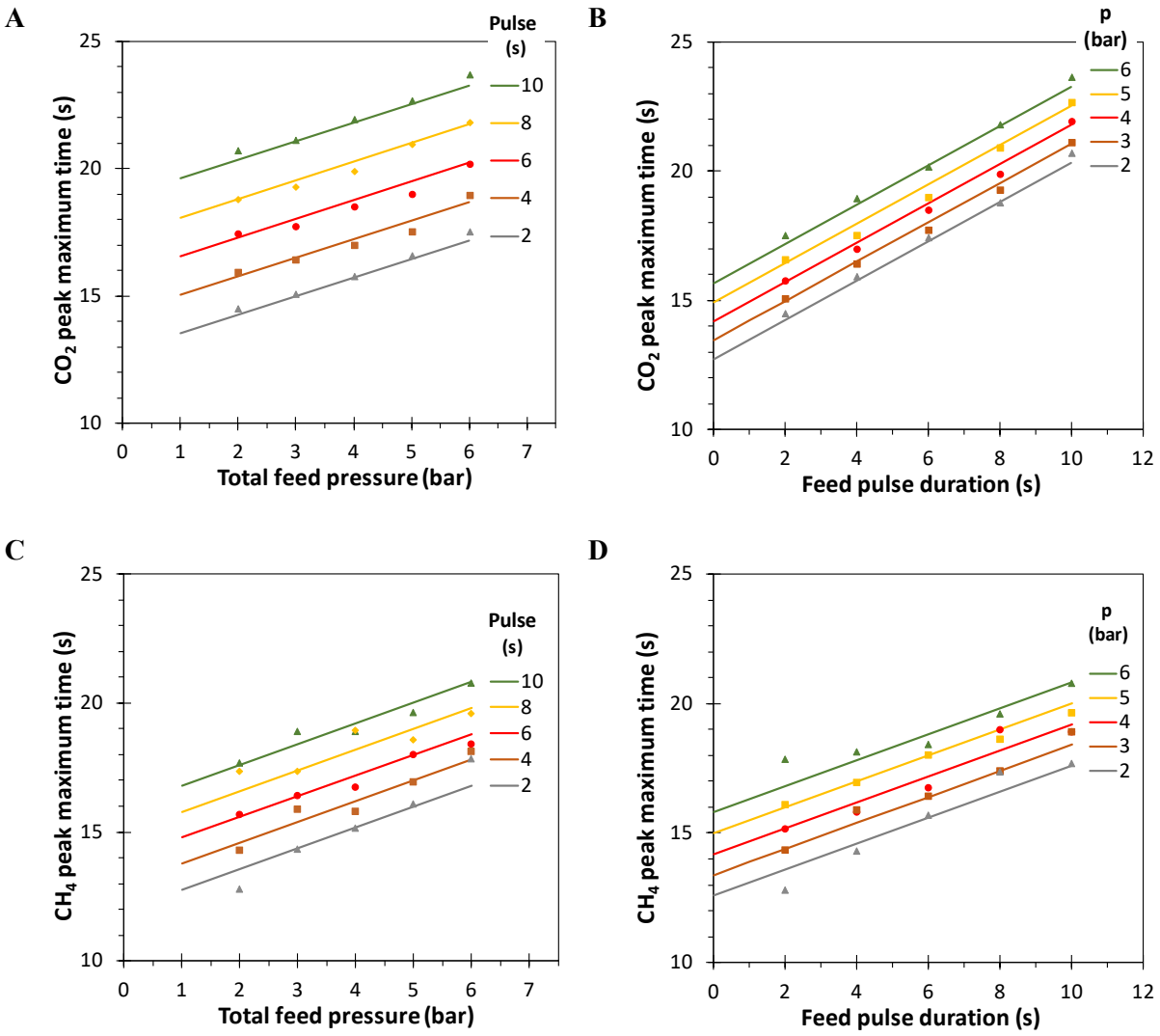

Figure 6. Time of peak maximum for CO_2 permeation (A,B) and CH_4 permeation (C,D) through the aluminium disk with pinhole as a function of pressure and pulse duration. The lines represent a least-squares fit with a linear trend in both time and pressure domain. The standard deviation of each individual point is far less than 0.5 s and the data can be described by the equations given in Table 1. The parity plot in Figure SI8 shows a good correlation between the measured and calculated values, especially for CO_2.

Table 1. Results of the least squares fit of the average instrumental residence time of CO_2 and CH_4 as a function of the feed pressure and the pulse time

Gas	Equation		Standard deviation [a)] (s)
CO_2	$\tau_{peak,CO2} = 11.27 + 0.761 \times t_{pulse} + 0.730 \times p_F$	Eq. 10	0.250
CH_4	$\tau_{peak,CH4} = 10.96 + 0.503 \times t_{pulse} + 0.805 \times p_F$	Eq. 11	0.426

[a] Standard deviation of all absolute errors in Figure 6

407

408 3.2.2.2. Analysis of the transport parameters of PDMS and PIM-DTFM-BTrip.

409 After identification of 6 s as a suitable pulse duration for the pinhole, an analogous test with the PDMS
410 membrane shows a much wider signal, due to the transient transport in the PDMS film itself (Figure SI9).
411 Qualitatively there is no significant effect of the pulse duration on the peak position from 2-10 s, while only at
412 a pulse duration of 2 s, the peak intensity becomes rather low. This confirms the 6 s pulse to be a good choice.
413 The peak width of the pinhole is virtually negligible to that of the PDMS membrane, suggesting that the
414 instrumental residence time is not expected to affect significantly the shape of the permeation curve for the
415 PDMS membrane. Figure 7 and Figure 8 show the permeation curves for a 6 s pulse of CO_2, CH_4 and their
416 35/65 vol.% mixture in the PDMS film and the PIM-DTFM-BTrip film, respectively at pressures from 1 to 6
417 bar(a).

418 The instrumental response is much faster than that of the PDMS film and the signal of the pinhole in the
419 aluminium film is almost negligible, both in time and in peak width. Therefore, the PDMS peak shape is not
420 significantly affected by the instrumental setup, and subtraction of the average instrumental residence time
421 (Eq. 10 and Eq. 11) from the time axis, should allow fitting of the entire curve with Eq. A11 to calculate all
422 transport parameters *P*, *D* and *S*. On the other hand, the response of the pinhole is only slightly faster than that
423 of the PIM-DTFM-BTrip film, especially for CO_2, and therefore the signal is likely so much deformed that a
424 fit of the entire curve is not possible if the peak broadening due to the instrument itself is not considered.
425 Qualitatively, there is no obvious difference between the peak shape and position in the pure and the mixed
426 gas permeation measurements, with exception of the higher noise for the mixtures due to the lower signal.
427 There is a weak increase in the peak position with increasing pressure, which is best visible for the PIM that
428 has the shortest time scale, but this is probably mostly due to the effect discussed in Figure 6. In all curves, the
429 peak height increases more or less proportionally with the pressure, because upon substitution of $t = \tau_{Max} =$
430 $\frac{l^2}{10.9D}$, Eq. A11 becomes independent of time and increases linearly with the feed pressure.

431

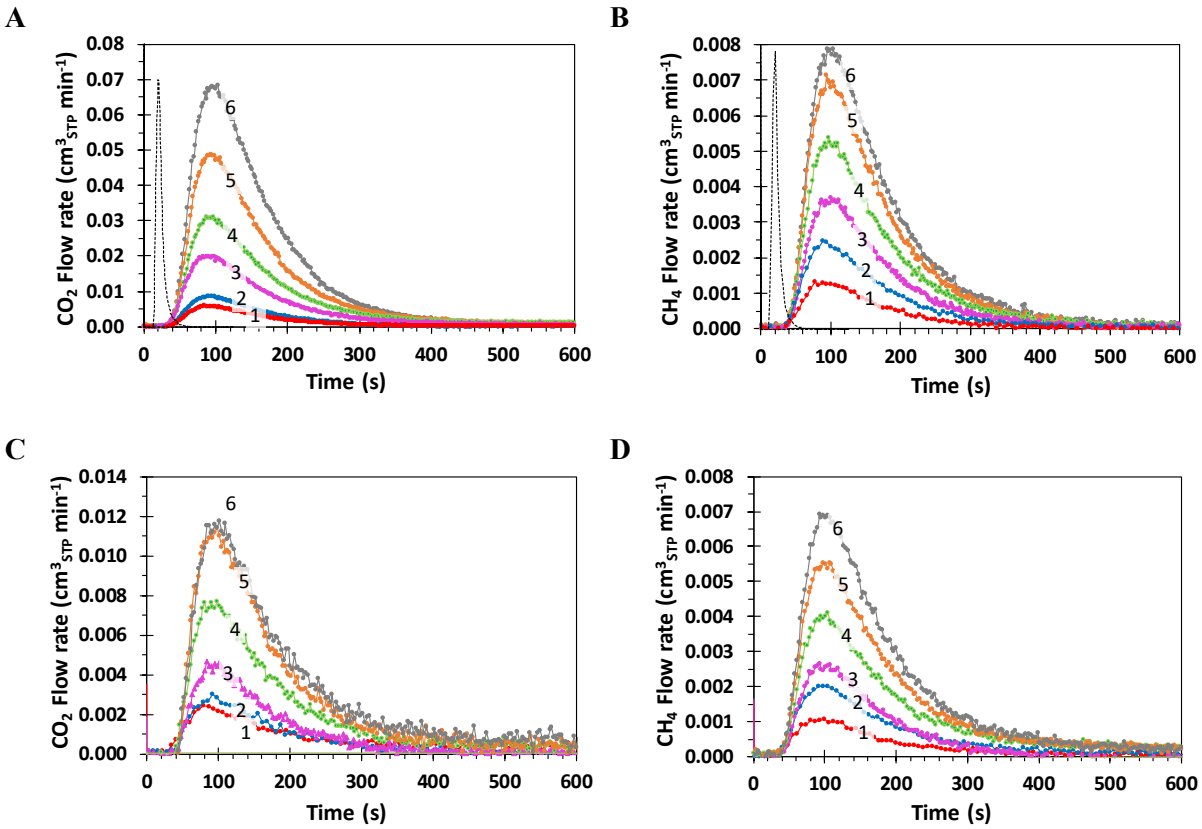

Figure 7. Permeate flow rate of pure CO_2 (A), pure CH_4 (B) and the same gases using a 35/65 vol% CO_2/CH_4 mixture (C,D) after a 6 s pulse and a feed flow rate of 500 cm^3_{STP} min^{-1} through the PDMS membrane (membrane thickness 1056 µm, effective area 13.84 cm^2). The numbers indicate the feed pressure in bar(a). A background of 3 vol% CO_2 and 3 vol% CH_4 in argon is used to guarantee a slightly higher baseline signal and correspondingly higher sampling rate. The dotted grey curves in the graph for pure CO_2 and pure CH_4 show for comparison the corresponding response of a 6 s pulse at 6 bar through the pinhole, scaled vertically to fit in the same graph.

432

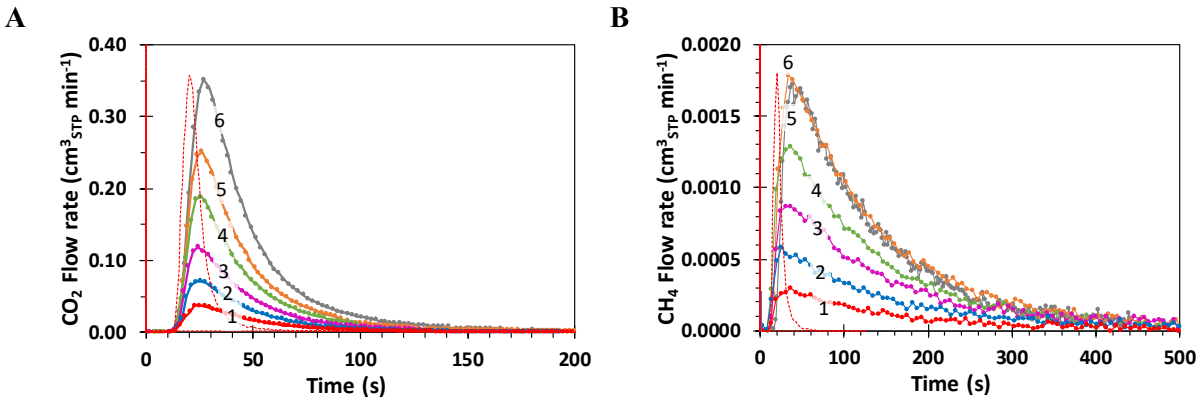

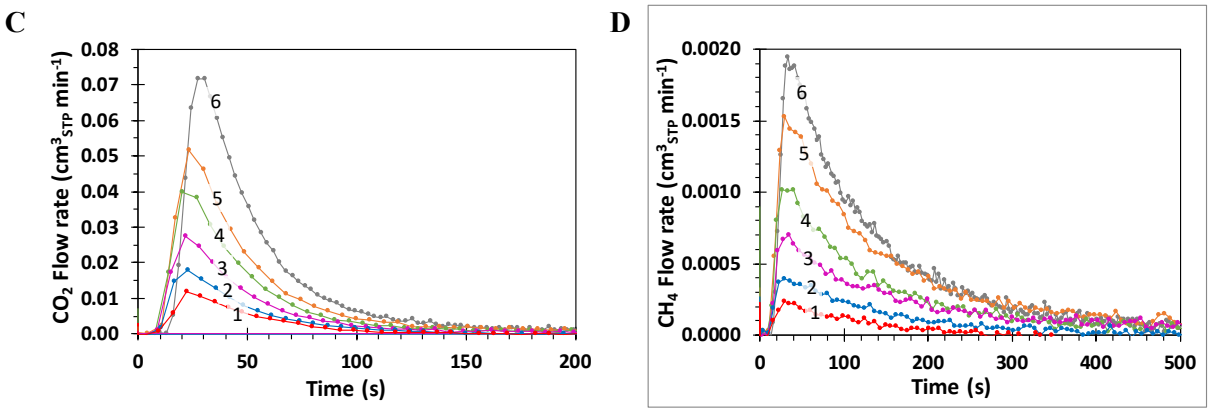

Figure 8. Permeate flow rate of pure CO_2 (A), pure CH_4 (B) and the same gases using a 35/65 vol% CO_2/CH_4 mixture (C,D) after a 6 s pulse and a feed flow rate of 500 cm^3_{STP} min^{-1} through the PIM-DTFM-BTrip membrane (membrane thickness 112 ± 6 µm, effective area 0.785 cm^2, age 1382 days + max 5 days to complete the measurement cycle). The numbers indicate the feed pressure in bar(a). A background of 3 vol% CO_2 and 3 vol% CH_4 in argon is used to guarantee a slightly higher baseline signal and correspondingly higher sampling rate. The dotted red curve in the graphs for pure CO_2 and pure CH_4 show for comparison the corresponding response of a 6 s pulse at 6 bar through the pinhole, scaled vertically to fit in the same graph.

The pulse peak position is very similar for the PIM and for the pinhole, but the PIM signal is clearly much wider. This suggests that the estimation of the diffusion coefficient can still be relatively accurate, because the membrane has the largest influence on the overall signal. Since the complete fit of the permeation curve is not possible for the PIM, only the peak maximum was determined by a partial fit of the peak apex, and the maximum due to the membrane transport, $\tau_{Max,Mem}$ was determined as follows:

$$\tau_{Max,Mem} = \tau_{Max} - \tau_{Max,0} \qquad \text{Eq. 12}$$

Where $\tau_{Max,0}$ is the peak position of system response, *i.e.* of the pulse on the aluminium sample with pinhole given by Eq. 10 and Eq. 11. The diffusion coefficient is than calculated by rearrangement of Eq. A12 as:

$$D = \frac{l^2}{10.9\,\tau_{Max,Mem}} \qquad \text{Eq. 13}$$

The results are plotted in Figure 9. There is some scatter in the diffusion data, which does not allow to identify an unambiguous trend as a function of the feed pressure or a difference between pure and mixed gas diffusion coefficients in PDMS. Instead, in the PIM, both CO_2 and CH_4 have a higher diffusion coefficient in the mixed gas experiment than in the pure gas experiment. The standard mixture (Ar with 3 vol.% of CO_2 and 3 vol.% of CH_4) that is used as the background has apparently little effect on the diffusion coefficient because of the low CO_2 partial pressure. The average values of the diffusion coefficient taken at all pressures lie remarkably close to the values determined by the other methods (Table 2 and Table 3), confirming the validity of the procedures. For a more sensitive determination of the effect of the gas pressure or composition, CO_2

449 could be run at the background when making CH_4 pulses and vice versa, or ^{13}C labelled CO_2 and CH_4 could
450 be used for the pulse while the unlabelled mixture is permeating.
451

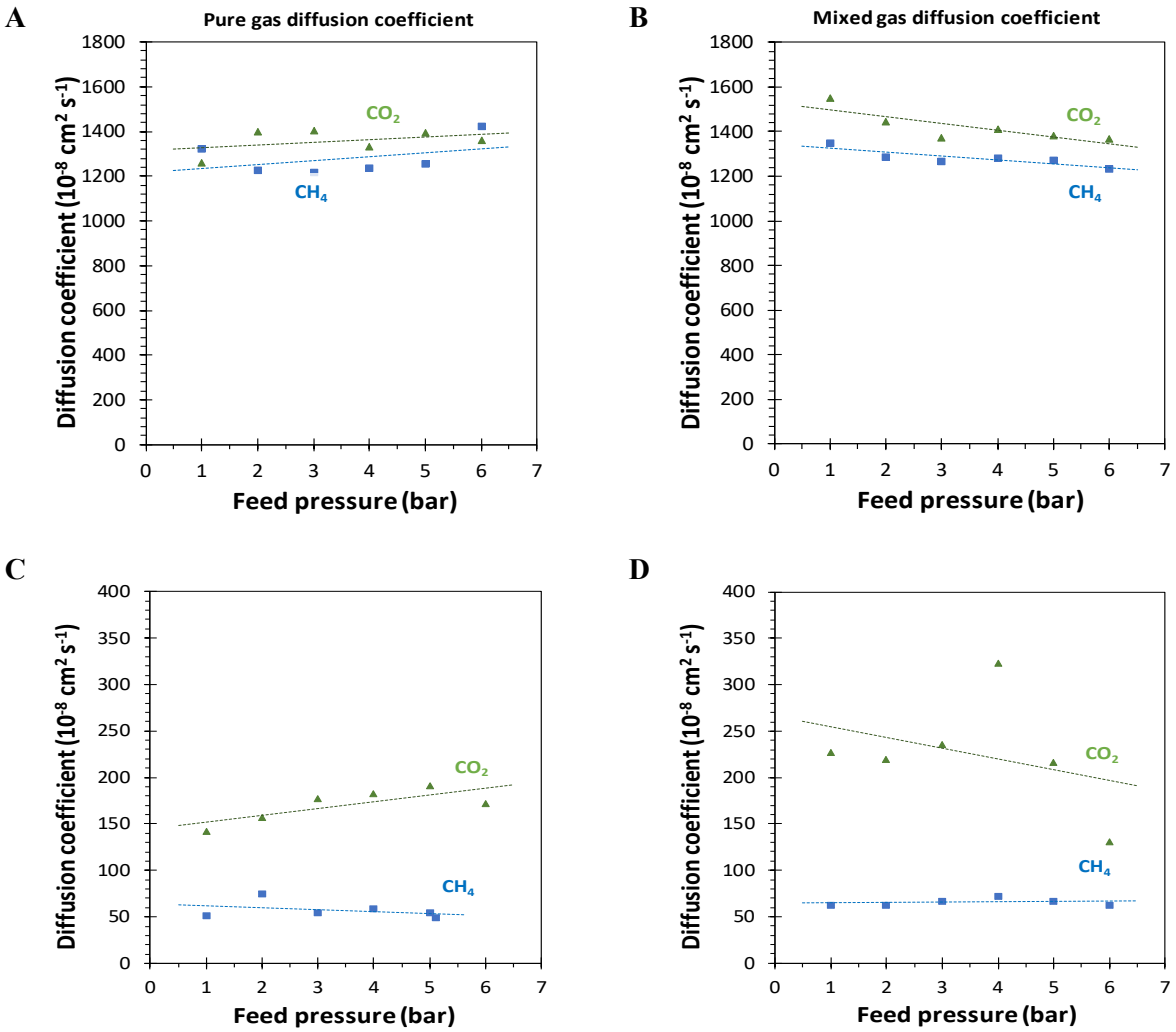

Figure 9. Diffusion coefficients for pure CO_2 and CH_4 (A,C) and for a 35/65 vol.% CO_2/CH_4 mixture (B,D) in a 1056 µm thick PDMS film (top) and a 112 µm thick PIM-DTFM-BTrip film (bottom) as a function of the feed gas pressure. Feed gas mixture of 3 vol.% CO_2 and 3 vol.% CH_4 in Argon, followed by a 6 second pulse of the gas or gas mixture of interest. The lines are plotted as a guide to the eye. PIM-DTFM-BTrip membrane age 1382 days (+ max. 5 to complete the measurement cycle).

452

453 *3.3. Comparison of methods*

454 An overview of the results for all different methods is given in Table 2 for PDMS and Table 3 for PIM-
455 DTFM-BTrip, while a selected number of data is also plotted in the Robeson diagram (Figure 10). Despite the
456 different instruments used and despite the different measurement and evaluation modes when using the same
457 instrument, the transport parameters of CO_2 and CH_4 in PDMS are strikingly similar, with a maximum of
458 around 10% spread in both the permeability and the diffusion coefficient. Regardless the method used, the

mixed gas diffusion coefficient of methane is systematically higher than the single gas diffusion coefficient, but there is no systematic trend for CO_2.

Table 2. Transport properties P, D and S with the corresponding selectivities P_a/P_b, D_a/D_b, S_a/S_b for PDMS.

	P_a [Barrer = 10^{-10} cm^3_{STP} cm cm^{-2} s^{-1} $cmHg^{-1}$]						Selectivity α_P (P_a/P_b)			
	N_2	O_2	CO_2	CH_4	H_2	He	H_2/N_2	CO_2/N_2	O_2/N_2	CO_2/CH_4
Fixed Vol. Tangent	235	501	2628	747	508	273	2.16	11.2	2.14	3.52
Fixed V Complete fit	235	499	2632	747	509	274	2.16	11.2	2.14	3.52
Variable Vol. Tangent			2802	955						2.9
(mixed gas)			(2815)	(894)						(3.1)
Complete fit tangent			3028	894						3.4
(mixed gas)			(2271)	(1051)						(2.2)
Complete fit sigmoidal			3028	894						3.4
(mixed gas)			(2275)	(1051)						(2.2)
	D_a [10^{-12} m^2s^{-1}]						Selectivity α_D (D_a/D_b)			
	N_2	O_2	CO_2	CH_4	H_2	He	H_2/N_2	CO_2/N_2	O_2/N_2	CO_2/CH_4
Fixed Vol. Tangent	1461	1777	1441	1274	5050	6889	3.46	0.99	1.22	1.13
Fixed V Complete fit	1469	1784	1423	1260	5107	6954	3.48	0.97	1.21	1.13
Variable Vol. Tangent			1652	1391						1.19
(mixed gas)			(1516)	(1671)						(0.91)
Complete fit tangent			1429	1290						1.11
(mixed gas)			(1396)	(1443)						(0.97)
Complete fit sigmoidal			1432	1293						1.11
(mixed gas)			(1399)	(1428)						(0.98)
Pulse method			1393 ±31	1279 ±80						1.08
(mixed gas)			(1422±68)	(1282 ±39)						(1.11)
	S_a [cm^3 cm^{-3} bar^{-1}]						Selectivity α_S (S_a/S_b)			
	N_2	O_2	CO_2	CH_4	H_2	He	H_2/N_2	CO_2/N_2	O_2/N_2	CO_2/CH_4
Fixed Vol. Tangent	0.12	0.21	1.37	0.44	0.08	0.03	0.66	11.4	1.75	3.11
Fixed V Complete fit	0.12	0.21	1.39	0.44	0.07	0.03	0.58	11.6	1.75	3.16
Variable Vol. Tangent			1.27	0.51						2.49
(mixed gas)			(1.39)	(0.40)						(3.47)
Complete fit tangent			1.59	0.52						3.06
(mixed gas)			(1.22)	(0.55)						(2.22)
Complete fit sigmoidal			1.58	0.52						3.04
(mixed gas)			(1.22)	(0.55)						(2.22)

Table 3. Transport properties P, D and S with the corresponding selectivities P_a/P_b, D_a/D_b, S_a/S_b for PIM-DTFM-BTrip.

	Age [a]	P_a [Barrer = 10^{-10} cm^3_{STP} cm cm^{-2} s^{-1} $cmHg^{-1}$]						Selectivity α_P (P_a/P_b)			
	(days)	N_2	O_2	CO_2	CH_4	H_2	He	H_2/N_2	CO_2/N_2	O_2/N_2	CO_2/CH_4
Fixed Vol. Tangent	274	729	3048	14376	719	9654	4483	13.2	19.7	4.18	20.0
Fixed V Complete fit	274	728	3097	14497	722	9648	4531	13.2	19.9	4.28	20.1
Variable Vol. Tangent (mixed gas)	1384			18049 (19297)	1141 (1167)						15.1 (16.5)
Complete fit tangent (mixed gas)	1384			17854 (18673)	1120 (1220)						15.9 (15.3)
Complete fit sigmoidal (mixed gas)	1384			17940 (18601)	1115 (1214)						16.1 (15.3)
	Age [a]	D_a [10^{-12} m^2s^{-1}]						Selectivity α_D (D_a/D_b)			
	(days)	N_2	O_2	CO_2	CH_4	H_2	He	H_2/N_2	CO_2/N_2	O_2/N_2	CO_2/CH_4
Fixed Vol. Tangent	274	114	474	171	32.1	8635	9465	75.7	1.50	4.16	5.33
Fixed V Complete fit	274	125	488	179	34.2	9078	12210	72.6	1.43	3.90	5.23
Variable Vol. Tangent (mixed gas)	1384			92.7 (170)	54.5 (55.0)						1.70 (3.09)
Complete fit tangent (mixed gas)	1384			94.9 (193)	58.6 (58.4)						1.61 (3.30)
Complete fit sigmoidal (mixed gas)	1384			91.5 (193)	62.2 (60.2)						1.47 (3.20)
Pulse method (mixed gas)	1384			170 ±18 (226 ±61)	57 ± 9 (66 ±4)						2.98 (3.43)
	Age [a]	S_a [cm^3_{STP} cm^{-3} bar^{-1}]						Selectivity α_S (S_a/S_b)			
	(days)	N_2	O_2	CO_2	CH_4	H_2	He	H_2/N_2	CO_2/N_2	O_2/N_2	CO_2/CH_4
Fixed Vol. Tangent	274	4.80	4.82	63.2	16.8	0.84	0.36	0.17	13.2	1.00	3.76
Fixed V Complete fit	274	4.36	4.75	60.6	15.8	0.79	0.27	0.18	13.9	1.09	3.83
Variable Vol. Tangent (mixed gas)	1384			167 (84.7)	18.8 (15.6)						8.88 (5.43)
Complete fit tangent (mixed gas)	1384			141 (88.8)	14.3 (15.6)						9.86 (5.69)
Complete fit sigmoidal (mixed gas)	1384			147 (72.4)	13.4 (15.1)						10.9 (4.79)

[a] Membrane age after MeOH treatment, plus up to 5 days after the indicated age to complete the measurement cycle.

For PIM-DTFM-Btrip, there is somewhat more spread in the data. In terms of permeability, the variable volume setup gives higher permeabilities than the fixed volume setup for both CO_2 and CH_4, for all the methods used. However, the variable volume setup gives lower pure gas diffusion coefficients for CO_2 than the fixed volume setup, but very similar mixed gas diffusion coefficients, while the diffusion coefficients are substantially higher in the variable volume setup with all three measurement modes, both for the pure gases

and for the mixed gases. The latter demonstrates the presence of a positive coupling effect of CO_2 for CH_4, while the lower pure gas diffusivity of CO_2 indicates a negative coupling by CH_4.

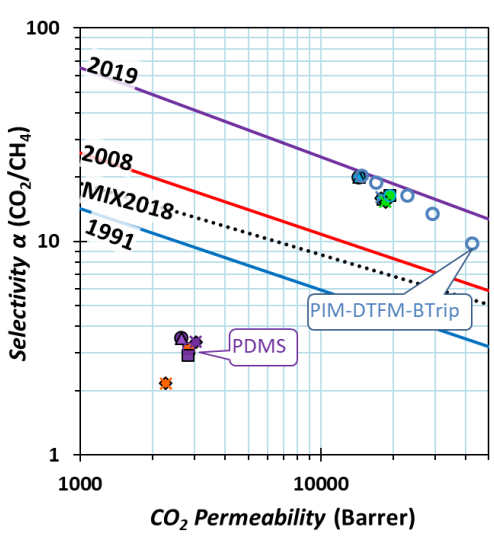

Figure 10. Robeson plot with an overview of the results for the CO_2/CH_4 gas pair in PDMS (Table 2) and PIM-DTFM-BTrip (Table 3). Data for PDMS are reported in purple for single gas and orange for mixed gas, while data for PIM-DTFM-BTrip are reported in blue for single gases and green for mixed gas. Symbols shapes indicate the different instrument or method used for their analysis: Fixed Volume Tangent (●), Fixed Volume Complete fit (■), Variable Volume Tangent (▲), Variable Volume, Complete fit time lag curve (◆), Variable Volume, Complete fit sigmoidal curve (X). Empty blue symbols indicate change in separation performance as a function of aging time for the PIM-DTFM-BTrip (data from Ref. [16])

3.4. Gas separation process evaluation

In real separation processes, the membranes normally operate under steady state conditions, where the most important variables are the feed pressure and the feed gas composition. While the transient measurements proved useful for the analysis of the transport parameters, yielding detailed information on the transport mechanism and its anomalies, Figure 11 shows an overview of the results under stationary conditions with the comparison of pure and mixed gas permeability and selectivity for both polymers as a function of the total feed pressure (A,B and D,E) and feed composition (C,F). PDMS shows negligible pressure dependence in the range

of 1-6 bar absolute pressure at 35 vol% of CO_2 in methane, and also very low composition dependence in the range of 10-50 vol% of CO_2 in methane at 6 bar(a) feed pressure. While it was shown in the previous sections that the diffusion of CH_4 is slightly faster in the mixture in both PDMS and the PIM (Figure 4), the CH_4 mixed gas permeability is somewhat lower than the pure gas permeability, and CO_2 is unaffected, and thus the CO_2/CH_4 selectivity results slightly higher than the ideal selectivity. This is apparently due to competitive sorption of CO_2 and CH_4, which reduces the solubility of the CH_4.

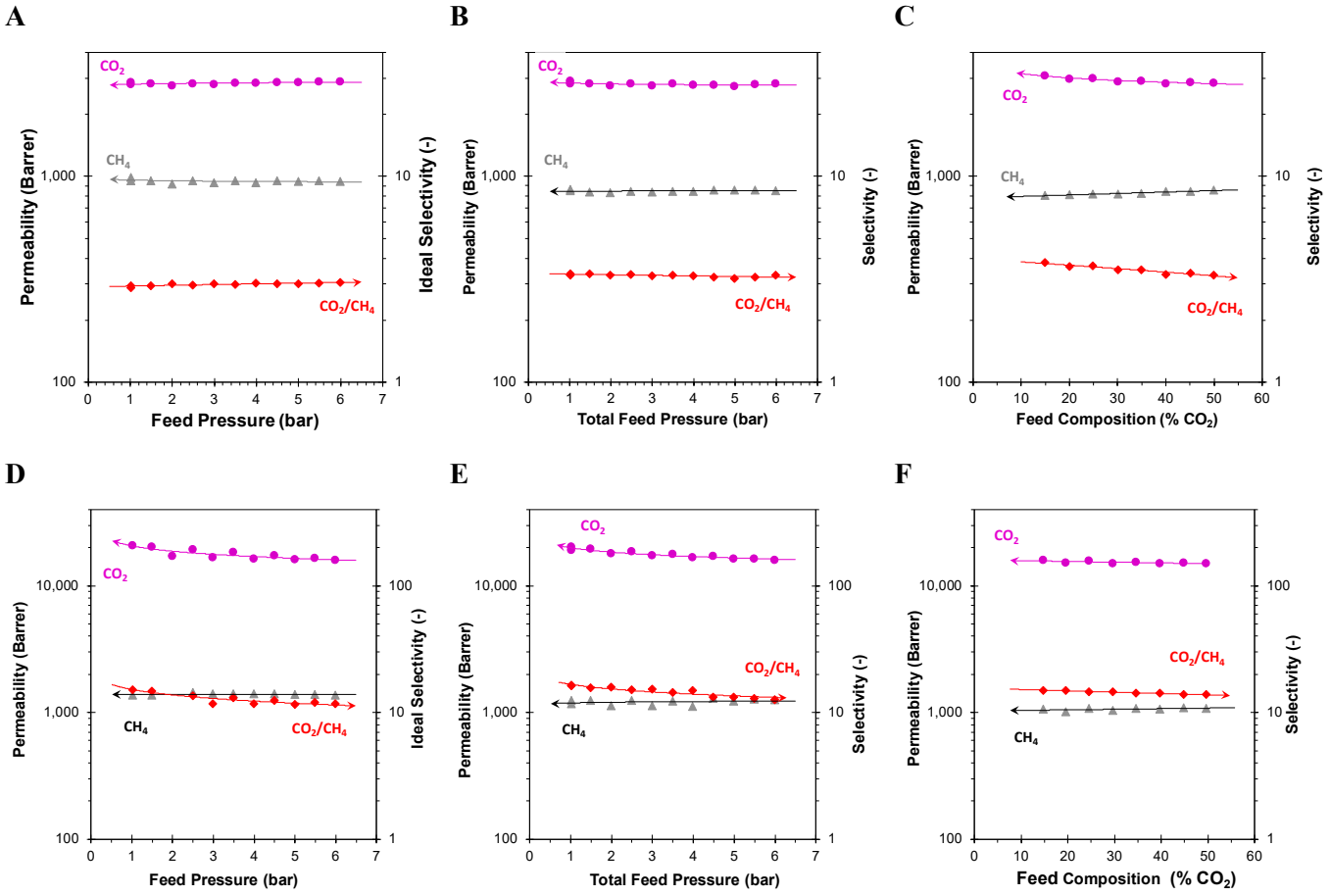

Figure 11. Permeability (in Barrer) of pure CO_2 and CH_4 as a function of the feed pressure in (A) PDMS and (D) PIM-DTFM-BTrip. Corresponding curves (B,E) for mixed gas permeation with a 35/65 vol% CO_2/CH_4 and (C,F) plot of the composition-dependence at 6 bar(a) feed pressure. The lines serve as a guide to the eye only. The symbols at integer values of pressure and at 10, 20, 30, 40 and 50% CO_2 represent the increasing pressure steps or CO_2 concentration in the feed, while the points at half-integer value of pressure or the points at 15, 25, 35 and 45 % CO_2 represent the subsequent decreasing pressure steps or CO_2 concentration. The arrowheads on the lines point towards the axis where to read the data. Membrane age 274 days (+ max. 5 days to complete the measurement cycle).

There is no evidence of plasticization by CO_2, which generally occurs at higher CO_2 partial pressure, and is more evident in glassy polymers than in rubbers. Opposite to PDMS, the sample of PIM-DTFM-BTrip shows a distinct pressure dependence for CO_2 permeation, while the CH_4 permeability is nearly constant as a function of the feed pressure (Figure 11 D,E). As a result, the ideal selectivity and the mixed gas selectivity

492 decreases with increasing pressure, according to a similar trend. At a total pressure of 6 bar(a), instead, the
493 composition-dependence is almost negligible. In all three experiments there is also some hysteresis between
494 the increasing and decreasing pressure (Figure 11D,E) or CO_2 concentration (Figure 11F), with the highest
495 values being recorded in the (partial) pressure decrease run. The hysteresis in the PIM sample suggests that
496 dilation occurs at the highest absolute pressure or CO_2 partial pressure, which does not relax back to the original
497 volume within the duration of a measurement cycle and therefore the permeability increases. Indeed, the effect
498 is strongest for the pure gas permeation measurements, where the CO_2 partial pressure reaches 6 bar(a), while
499 it reaches a maximum of 2.1 bar for the measurements at variable pressure (Figure 11E) and 3.0 bar for the
500 measurements at variable composition (Figure 11F). The pressure-dependence of the permeability in the PIM
501 is in line with the results above and confirms that it is strictly not possible to describe the transport in the PIM
502 with simple Fickian diffusion. Under the same conditions, PIM-DTFM-BTrip shows systematic much higher
503 permeability at different feed pressures with respect to PIM-2 [28] and PIM-SBF-1 [64], and also higher
504 permeability with respect to the ultrapermeable PIM-SBI-Trip [81], even if the latter as a higher selectivity
505 positioning both of them close to the most recent upper bounds. Given its fluorinated nature, it might be
506 expected that the performance of PIM-DTFM-Trip is less affected by the presence of humidity, similarly to
507 what was observed for PIM-2 [28]. This makes this PIM of interest for further studies regarding industrial
508 separations where large quantities of humid gases must be treated.
509

510 **4. Conclusions**

511 The present paper describes the detailed analysis of the transient phase of mixed gas transport through two
512 fundamentally different membrane materials, namely the glassy benzotriptycene-based ultrapermeable
513 polymer of intrinsic microporosity (PIM-DTFM-BTrip) and the rubbery polydimethylsiloxane (PDMS), via
514 the online analysis of the permeate gas composition and flow rate by means of a mass-spectrometric residual
515 gas analyser. This analyser offers the unique advantage that it allows the calculation of the mixed gas diffusion
516 coefficients of all individual gases present in the mixture, thus providing novel insight into the transport in
517 these materials. The use of three different approaches (integral, differential and pulse signal) to determine the
518 mixed gas transport parameters, and the comparison with the 'classical' time lag method in a fixed volume
519 setup, provides further insight into the behaviour of the materials and in the strengths and limitations of the
520 different instruments and elaboration methods. The computational analysis of the entire permeation curve is
521 laborious, but provides the best insight in the gas transport mechanism, and unequivocally reveals non-Fickian
522 behaviour, if present, via the deviation of the experimental results from the theoretical permeation curve. It
523 also confirms the well-known but generally ignored limitations of the traditional time lag measurements, which
524 measures the effective transport parameters, but does not consider anomalies such as non-Fickian diffusion.
525 On the other hand, the time lag and other singular points provide the simplest and fastest methods for
526 determining the effective diffusion coefficient of gases in membranes.
527 All three approaches used with the variable volume instrument showed very similar results for PDMS, with
528 a maximum of around 10 % spread in both the permeability and the diffusion coefficient compared to the

529 'standard' fixed volume method. The generally good fit of the permeation curves confirms both the reliability
530 of the methods, and the 'normal' behaviour of PDMS, ascribed to its thermodynamic equilibrium state in the
531 rubber phase, which is not subject to physical aging. The PIM shows strongly non-Fickian transport, unlike
532 that usually observed in rubbery or common glassy polymer membranes, with a very poor fit of the
533 experimental data with the theoretical permeation curves for simple Fickian diffusion and Henry type sorption,
534 indicating the presence of strongly pressure-dependent permeability and diffusion coefficients. PIM-DTFM-
535 BTrip further shows an evident coupling effect between CO_2 and CH_4 in mixed gas permeation experiments,
536 with a strong increase of the diffusion coefficient of CO_2 in the presence of CH_4 but a slightly weaker decrease
537 of its solubility. Interestingly, this PIM seems to have stopped aging after the 636 days reported in our previous
538 study [16] and was not affected by the measurements with gas mixtures at elevated CO_2 partial pressures up
539 to 6 bar(a).
540 All methods confirm to be suitable for the analysis of the diffusion coefficient of mixed gases. For future
541 work, the addition of an automatic gas switch after the mass flow controllers, could increase the reaction rate
542 of the system, and thus the accuracy of the results, by the generation of an instantaneous pulse or step change
543 in the feed gas. In order to fit the permeation curve correctly, especially for samples with a very short transient
544 phase, a correction for the signal broadening due to the instrument would be needed in addition to the correction
545 for the total response time.
546

547 **5. Appendix A: Mathematical models describing different permeation modes**

548 Numerous articles, books and book chapters have been dedicated to the mathematical description of the gas
549 transport through membranes, e.g. [14,82,83]. The models have an analytical solution for flat sheet membranes,
550 provided that a number of conditions are satisfied, such as a constant solubility and diffusivity of the gas in
551 the membrane material. The amount of gas permeating through the membrane can be described by a Tailor
552 series and the precise equation depends on whether we look at the permeation rate every moment or at the
553 cumulative amount of gas permeated. The sections below will describe the models for the instruments and the
554 specific procedures that we will use in this work.

555 *5.1. Fixed volume setup*

556 A typical time lag curve of the permeate pressure or total gas volume in a fixed volume is shown in Figure
557 A1A. Under the boundary conditions of concentration-independent solubility and diffusion coefficient,
558 constant feed pressure, the absence of any gas dissolved inside the membrane before the experiment, and
559 negligible permeate pressure compared to the feed, the trend of the total amount of gas in the permeate has an
560 analytical solution. For the fixed-volume setup used in this work, the pressure p_t as a function of time t through
561 a membrane with thickness l can be described as [63,84]:

Eq. A1

$$\left(\frac{dp}{\quad}\right) \quad \frac{RT}{\quad}$$

$$\cdot\left(\frac{D\cdot t}{l^2}-\frac{1}{6}-\frac{2}{\pi^2}\sum_{n=1}^{\infty}\frac{(-1)^n}{n^2}\exp\left(-\frac{D\cdot n^2\cdot\pi^2\cdot t}{l^2}\right)\right)$$

where p_0 and $(dp/dt)_0$ are the starting pressure and the baseline slope, respectively, which should be negligible in a well-evacuated and leak free membrane and permeability instrument. R is the universal gas constant [$8.314\cdot10^{-5}$ m^3 bar $mol^{-1}\cdot K^{-1}$], T is the absolute temperature [K], A is the exposed membrane area [m^2], V_P is the permeate volume [m^3], V_m the molar volume of a gas at standard temperature and pressure [$22.41\cdot10^{-3}$ m^3_{STP} mol^{-1} at 0°C and 1 atm], p_f the feed pressure [bar], S the gas solubility [m^3_{STP} m^{-3} bar^{-1}] and D the diffusion coefficient [m^2 s^{-1}]. Converting the pressure in the fixed volume permeate side to a permeate volume at standard temperature and pressure, V_{STP}, the following terms must be substituted in Eq. A1:

$$p_t = V_{t,STP}\frac{p_{STP}\times T}{V_P\,T_{STP}} \qquad \text{Eq. A2}$$

$$p_0 = V_{0,STP}\frac{p_{STP}\times T}{V_P\,T_{STP}} \qquad \text{Eq. A3}$$

$$\left(\frac{dp_t}{dt}\right)_0 = \left(\frac{dV_t}{dt}\right)_{0,STP}\times\frac{p_{STP}\times T}{V_P\,T_{STP}} \qquad \text{Eq. A4}$$

Thus, V_{STP} at any time becomes:

$$V_{t,STP} = V_{0,STP} + \left(\frac{dV_t}{dt}\right)_{0,STP}\cdot t + \frac{RT_{STP}}{p_{STP}V_m}\cdot A\cdot l\cdot p_f\cdot S \cdot\left(\frac{D\cdot t}{l^2}-\frac{1}{6}-\frac{2}{\pi^2}\sum_{n=1}^{\infty}\frac{(-1)^n}{n^2}exp\left(-\frac{D\cdot n^2\cdot\pi^2\cdot t}{l^2}\right)\right) \qquad \text{Eq. A5}$$

Where $\frac{RT_{STP}}{p_{STP}V_m}=1$ and can be ignored.

5.1.1. Tangent time lag method

The tangent method is the most commonly used method to calculate the diffusion coefficient from the steady state gas permeation curve. For long times, the pressure-increase rate or the volumetric flow rate become constant, and Eq. A1 and Eq. A5 reduce to:

$$p_t = \frac{RT}{V_pV_m}\frac{A\cdot p_f\cdot S\cdot D}{l}\left(t-\frac{l^2}{6D}\right) \qquad \text{Eq. A6}$$

$$V_{t,STP} = \frac{A\cdot p_f\cdot S\cdot D}{l}\left(t-\frac{l^2}{6D}\right) \qquad \text{Eq. A7}$$

which both describe a straight line (shown for p_t in Figure A1), that intersects the horizontal axis at the time defined as the time lag Θ or τ_L:

$$t = \frac{l^2}{6D} \equiv \Theta \text{ or } \tau_{TL} \qquad \text{Eq. A8}$$

Measurement of the time lag allows for the calculation of the experimental diffusion coefficient via Eq. A8, if the membrane thickness is known.

5.1.2. *Integral fit of the pressure-increase curve (fixed volume setup)*

The tangent method requires that the permeation reaches a pseudo-steady state, from where the tangent can be extrapolated to the time axis. If the steady state is not reached, for instance in relatively thick membranes or for permeants with a low diffusion coefficient and high solubility, for which the measurement time is extremely long, then a least-squares fit of the entire permeation curve may offer a solution [72]. In this case, Eq. A1 must be expanded in an appropriate number of terms that fits the experimental points and yields the values of P, D and S directly. If the curve shape deviates from the experimental points, this is an indication of anomalous transport, such as (partial) immobilization [33] or clustering of the permeating species [84], or plasticization of the polymer.

5.2. *Cross flow permeation cell (variable volume setup)*

The most common method to measure the permeation of gas mixtures uses a variable volume setup with a cross-flow permeation cell, and measures the volumetric permeate flow rate. Usually, the steady state flow rate J_∞ is determined directly by a flow meter, or indirectly via the concentration of the permeating gas in a sweeping gas stream with known flow rate. The steady state flow rate is given by the equation:

$$J_\infty = \frac{A \cdot (p_f - p_P) \cdot S \cdot D}{l} \qquad \text{Eq. A9}$$

If the partial pressure of the gas in the permeate is negligible (i.e. $p_P \ll p_f$), this corresponds to the slope of the time lag curve under steady state conditions (Eq. A7). Under the same boundary conditions (no gas present in the membrane before the experiment, permeate concentration negligible compared to the feed concentration), the transient gas flow rate from the moment when the membrane is first exposed to the gas is mathematically described by the derivative of the time lag curve in Eq. A5. It takes the form of a sigmoidal curve, described by the following equation:

$$\frac{dV_{t,STP}}{dt} = \left(\frac{dV_t}{dt}\right)_{0,STP} + A \cdot p_f \cdot S \cdot \frac{D}{l} \cdot \left(1 + 2\sum_{n=1}^{\infty} (-1)^n \, exp\left(-\frac{D \cdot n^2 \cdot \pi^2 \cdot t}{l^2}\right)\right) \qquad \text{Eq. A10}$$

Under normal conditions and in the absence of leaks in the system and in the membrane, the term $\left(\frac{dV_t}{dt}\right)_{0,STP}$ is negligible. Most cross-flow setups typically use periodic analysis of the gas composition by GC or micro GC, but with a sufficiently quick analyser one could also monitor the permeate flow rate continuously. It was previously reported that an online mass-spectrometric residual gas analyser can evaluate multiple gases at the same time, and integration of the signal allows the calculation of the mixed gas time lag, and thus mixed gas diffusion coefficients [60,63].

If the membrane is exposed to a short pulse of a gas in the feed (ideally a delta function with area = 1 and t << time lag), instead of a step-change, the flow rate of this gas in the permeate is described by the derivative of Eq. A10:

$$\left(\frac{dV_{t,STP}}{dt}\right)' = \left(\frac{dV_t}{dt}\right)'_{0,STP} - \frac{2D^2 \cdot \pi^2}{l^3} \cdot A \cdot p_f \cdot S \cdot \left(\sum_{n=1}^{\infty} n^2 \cdot (-1)^n \, exp\left(-\frac{D \cdot n^2 \cdot \pi^2 \cdot t}{l^2}\right)\right) \quad \text{Eq. A11}$$

This kind of experiment can be performed by flushing both sides of the cross-flow cell with a sweeping gas, briefly replacing it at the feed side with the gas or gas mixture of interest, and then following the flow rate of the gases in the permeate.

A plot of the signals according to Eq. A5, Eq. A10 and Eq. A11 is shown in Figure A1. The time lag in the integral curve, the inflection point in the differential curve and the peak maximum in the curve of the pulse, are characteristic times that depend on the diffusion coefficient and the membrane thickness. The analysis of these curves thus allows the calculation of *D* and *S*.

The inflection point in the differential curve corresponds to the peak maximum of the pulse and they are given by [68]:

$$\tau_{INF} = \tau_{Max} = \frac{l^2}{10.9D} \quad \text{Eq. A12}$$

Another characteristic time is the time needed in the differential method to reach half of the steady state permeate flow rate [68]:

$$\tau_{1/2} = \frac{l^2}{7.2D} \quad \text{Eq. A13}$$

Both times, also defined as 'singular points', can be used to calculate di diffusion coefficient if the membrane thickness is known. The area under the pulse corresponds to the steady state flow rate in the differential curve and should be proportional to the permeability. Thus, upon appropriate calibration, integration of the pulse signal should allow the calculation of the permeability.

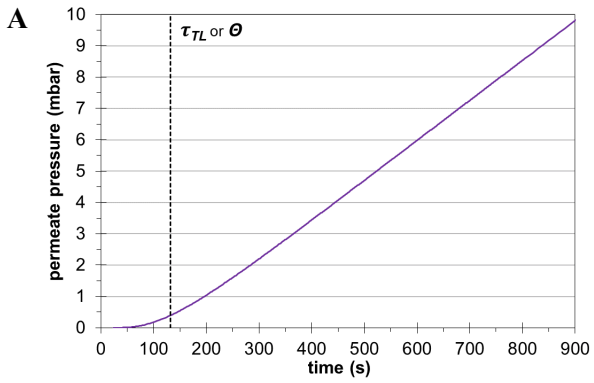

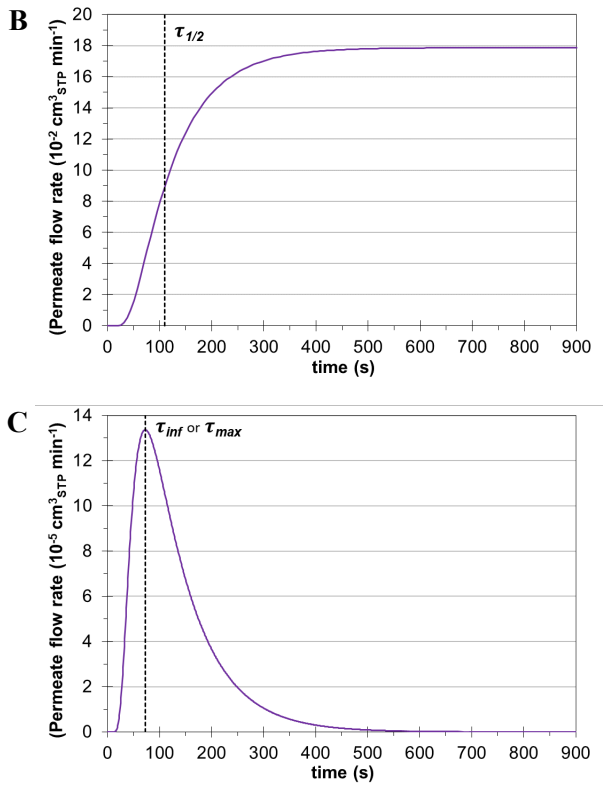

Figure A1. Plot of the permeate curves defined by (A) Eq. A5, (B) Eq. A10 and (C) Eq. A11 for a hypothetical membrane (area 10 cm^2, thickness 1000 μm) with a permeability of 3000 Barrer, a diffusion coefficient of 10^{-9} m^2 s^{-1} and a solubility of 2 cm^3_{STP} cm^{-3} bar^{-1} at a feed pressure of 1 bar.

5.3. Singular points method

In general, any of the singular points can be used to determine the diffusion coefficient of the penetrant:

$$D = \frac{l^2}{10.9\,\tau_{Max}} = \frac{l^2}{7.2\,\tau_{1/2}} = \frac{l^2}{6\,\tau_L} \qquad \text{Eq. A14}$$

Moreover, via the precise shape of the curves in Figure A1, defined by Eq. A5, Eq. A10 and Eq. A11, each of these singular points is directly related to the flow rate through the membrane, and thus to its permeability:

$$J_\infty = \frac{J(\tau_{Max})}{0.2442} = \frac{J(\tau_{1/2})}{0.5} = \frac{J(\tau_L)}{0.6266} \qquad \text{Eq. A15}$$

If the flow J_∞ is known and normalized, then the singular points can be easily determined via these relations and *vice versa*, measurement of the singular points allows calculation of J_∞. In the case of the pulse version, assuming the area of the peak $S = 1$, the flow rate can also be correlated with its height, h:

$$h = 0.5922\,J_\infty = 0.5922\,\frac{\pi^2 D}{l^2} \qquad \text{Eq. A16}$$

631 and for the peak width at half height, $\Delta_{(h/2)}$:

$$\Delta_{(h/2)} = 0.14025\frac{l^2}{\pi^2 D} \qquad \text{Eq. A17}$$

632 which allows simple determination of D. The singular points can be used as a criterion for the homogeneity
633 of the diffusion medium. In a homogeneous membrane, the diffusion coefficients calculated by any of formulas
634 in Eq. 5 will be the same, but in the presence of "facilitated" diffusion paths, the D values will decrease in the
635 order of time (see Eq. 5): $\tau_{Max} < \tau_{1/2} < \theta = \tau_{TL}$. Thus, the singular points provide the simplest and fastest method
636 for determining the diffusion coefficient of gases in membranes as a first approximation.
637

638 **Symbols and abbreviations**

Symbol	Parameter (unit)
A	Membrane area (cm^2)
c	Concentration ($cm^3_{STP}\ cm^{-3}$)
D	Diffusion coefficient ($cm^2\ s^{-1}$) or ($m^2\ s^{-1}$)
h	Peak height ($cm^3_{STP}\ s^{-1}$)
J	Flow rate ($cm^3_{STP}\ s^{-1}$)
l	Thickness (µm) or (cm) or (m)
p	Pressure (bar)
P	Permeability (Barrer = 10^{-10} cm^3_{STP} cm $cm^{-2}\ s^{-1}$ $cmHg^{-1}$)
R	Universal gas constant ($8.314\cdot10^{-5}$ m^3 bar $mol^{-1}\cdot K^{-1}$)
S	Solubility ($cm^3_{STP}\ cm^{-3}\ bar^{-1}$) or ($m^3_{STP}\ m^{-3}\ bar^{-1}$)
t	Time (s or min)
t_{pulse}	Pulse duration (s)
T	Absolute temperature (K)
V	Volume (cm^3) or (m^3)
V_m	Molar volume ($22.41\cdot10^{-3}$ $m^3_{STP}\ mol^{-1}$ at 0°C and 1 atm)
x	Coordinate (m) or (cm)
Greek symbol	
α	Selectivity (-)
Δ	Peak width (s)
Θ	Time lag (s)
Φ	Flow rate ($cm^3_{STP}\ s^{-1}$)
τ_{TL}	Time lag (s)
Subscript, index	
a	Gas species a
b	Gas species b
D	Diffusion
f, F	feed

GC	gas chromatography
h/2	at half height
i	Gas species i
INF	Inflection point
m	molar
Max	Maximum
Mem	Membrane
P	Permeate, permeability
peak	at peak maximum
pulse	pulse (for pulse duration)
S	Solubility
STP	standard temperature and pressure (here 0°C and 1 atm)
t	at time t
TL	at time lag
V	Volumetric
0	at reference time t=0 or pressure p=0
½	at half height
∞	at infinite

Abbreviation	
AMU	Atomic mass unit
GC	Gas chromatography
GRG	Generalized Reduced Gradient
MFC	Mass flow controller
MS	Mass spectrometry, mass spectrometric
NMR	Nuclear magnetic resonance
PDMS	Polydimethylsiloxane
PIM	Polymer of intrinsic microporosity
PIM-DTFM-BTrip	PIM with ditrifluoromethyl benzotriptycene side groups (the specific PIM in this work)
PTMSP	poly(trimethylsilylpropyne)
RGA	Residual gas analyzer

Declaration of competing interest

The authors declare that they have no known competing financial interests or personal relationships that could have appeared to influence the work reported in this paper.

Acknowledgements

Part of the work carried out for this manuscript received financial support from the Fondazione CARIPLO, programme “Economia Circolare: ricerca per un futuro sostenibile” 2019, Project code: 2019-2090, MOCA - Metal Organic frameworks and organic CAges for highly selective gas separation membranes and heavy metal capture devices.

References

[1] R.S. Murali, T. Sankarshana, S. Sridhar, Air Separation by Polymer-based Membrane Technology, Sep. Purif. Rev. 42 (2013) 130–186. doi:10.1080/15422119.2012.686000.

[2] N.W. Ockwig, T.M. Nenoff, Membranes for hydrogen separation, Chem. Rev. 107 (2007) 4078–4110. doi:10.1021/cr0501792.

[3] Air Products, Advanced Prism ® Membrane Systems For Cost Effective Gas Separations, 1999. http://www.airproducts.ru/~/media/Files/PDF/industries/membranes-supply-options-brochure-advanced-prism-membrane-systems.pdf.

[4] G. George, N. Bhoria, S. Alhallaq, A. Abdala, V. Mittal, Polymer membranes for acid gas removal from natural gas, Sep. Purif. Technol. 158 (2016) 333–356. doi:10.1016/j.seppur.2015.12.033.

[5] B. Kraftschik, W.J. Koros, J.R. Johnson, O. Karvan, Dense film polyimide membranes for aggressive sour gas feed separations, J. Membr. Sci. 428 (2013) 608–619. doi:10.1016/j.memsci.2012.10.025.

[6] P. Bernardo, E. Drioli, G. Golemme, Membrane Gas Separation: A Review/State of the Art, Ind. Eng. Chem. Res. 48 (2009) 4638–4663. doi:10.1021/ie8019032.

[7] M. Galizia, W.S. Chi, Z.P. Smith, T.C. Merkel, R.W. Baker, B.D. Freeman, 50th Anniversary Perspective: Polymers and Mixed Matrix Membranes for Gas and Vapor Separation: A Review and Prospective Opportunities, Macromolecules. 50 (2017) 7809–7843. doi:10.1021/acs.macromol.7b01718.

[8] E. Esposito, L. Dellamuzia, U. Moretti, A. Fuoco, L. Giorno, J.C. Jansen, Simultaneous production of biomethane and food grade CO2 from biogas: an industrial case study, Energy Environ. Sci. 12 (2019) 281–289. doi:10.1039/C8EE02897D.

[9] C.Y. Chuah, K. Goh, Y. Yang, H. Gong, W. Li, H.E. Karahan, M.D. Guiver, R. Wang, T.H. Bae, Harnessing filler materials for enhancing biogas separation membranes, Chem. Rev. 118 (2018) 8655–8769. doi:10.1021/acs.chemrev.8b00091.

[10] R. Khalilpour, K. Mumford, H. Zhai, A. Abbas, G. Stevens, E.S. Rubin, Membrane-based carbon capture from flue gas: A review, J. Clean. Prod. 103 (2015). doi:10.1016/j.jclepro.2014.10.050.

[11] A.M. Arias, M.C. Mussati, P.L. Mores, N.J. Scenna, J.A. Caballero, S.F. Mussati, Optimization of multi-stage membrane systems for CO2 capture from flue gas, Int. J. Greenh. Gas Control. 53 (2016) 371–390. doi:10.1016/J.IJGGC.2016.08.005.

[12] S. E. Kentish, 110th Anniversary: Process Developments in Carbon Dioxide Capture Using Membrane Technology, Ind. & Eng. Chem. Res. 0 (2019) null-null. doi:10.1021/acs.iecr.9b02013.

[13] J. Deng, Z. Huang, B.J. Sundell, D.J. Harrigan, S.A. Sharber, K. Zhang, R. Guo, M. Galizia, State of

the art and prospects of chemically and thermally aggressive membrane gas separations: Insights from polymer science, Polymer (Guildf). (2021) 123988. doi:10.1016/j.polymer.2021.123988.

[14] J.G. Wijmans, R.W. Baker, The solution-diffusion model: a review, J. Membr. Sci. 107 (1995) 1–21. doi:10.1016/0376-7388(95)00102-I.

[15] J.G. Wijmans, R.W. Baker, The Solution-Diffusion Model: A Unified Approach to Membrane Permeation, 2006. doi:10.1002/047002903X.ch5.

[16] B. Comesaña-Gándara, J. Chen, C.G. Bezzu, M. Carta, I. Rose, M.-C. Ferrari, E. Esposito, A. Fuoco, J.C. Jansen, N.B. McKeown, Redefining the Robeson upper bounds for CO2 /CH4 and CO2 /N2 separations using a series of ultrapermeable benzotriptycene-based polymers of intrinsic microporosity, Energy Environ. Sci. 12 (2019) 2733–2740. doi:10.1039/C9EE01384A.

[17] H. Yin, Y.Z. Chua, B. Yang, C. Schick, W.J. Harrison, P.M. Budd, M. Böhning, A. Schönhals, First Clear-Cut Experimental Evidence of a Glass Transition in a Polymer with Intrinsic Microporosity: PIM-1, J. Phys. Chem. Lett. 9 (2018) 2003–2008. doi:10.1021/acs.jpclett.8b00422.

[18] I. Rose, C.G. Bezzu, M. Carta, B. Comesaña-Gándara, E. Lasseuguette, M.C. Ferrari, P. Bernardo, G. Clarizia, A. Fuoco, J.C. Jansen, K.E. Hart, T.P. Liyana-Arachchi, C.M. Colina, N.B. McKeown, Polymer ultrapermeability from the inefficient packing of 2D chains, Nat. Mater. 16 (2017) 932–937. doi:10.1038/nmat4939.

[19] M. Longo, M.P. De Santo, E. Esposito, A. Fuoco, M. Monteleone, L. Giorno, B. Comesaña-Gándara, J. Chen, C.G. Bezzu, M. Carta, I. Rose, N.B. McKeown, J.C. Jansen, Correlating Gas Permeability and Young's Modulus during the Physical Aging of Polymers of Intrinsic Microporosity Using Atomic Force Microscopy, Ind. Eng. Chem. Res. 59 (2020) 5381–5391. doi:10.1021/acs.iecr.9b04881.

[20] A. Fuoco, C. Rizzuto, E. Tocci, M. Monteleone, E. Esposito, P.M. Budd, M. Carta, B. Comesaña-Gándara, N.B. McKeown, J.C. Jansen, The origin of size-selective gas transport through polymers of intrinsic microporosity, J. Mater. Chem. A. 7 (2019) 20121–20126. doi:10.1039/C9TA07159H.

[21] N.B. McKeown, P.M. Budd, Exploitation of Intrinsic Microporosity in Polymer-Based Materials, Macromolecules. 43 (2010) 5163–5176. doi:10.1021/ma1006396.

[22] Z.-X. Low, P.M. Budd, N.B. McKeown, D.A. Patterson, Gas Permeation Properties, Physical Aging, and Its Mitigation in High Free Volume Glassy Polymers, Chem. Rev. 118 (2018) 5871–5911. doi:10.1021/acs.chemrev.7b00629.

[23] L.M. Robeson, The upper bound revisited, J. Membr. Sci. 320 (2008) 390–400. doi:10.1016/j.memsci.2008.04.030.

[24] Y. Wang, X. Ma, B.S. Ghanem, F. Alghunaimi, I. Pinnau, Y. Han, Polymers of intrinsic microporosity for energy-intensive membrane-based gas separations, Mater. Today Nano. 3 (2018) 69–95. doi:10.1016/J.MTNANO.2018.11.003.

[25] R. Swaidan, B. Ghanem, I. Pinnau, Fine-Tuned Intrinsically Ultramicroporous Polymers Redefine the Permeability/Selectivity Upper Bounds of Membrane-Based Air and Hydrogen Separations, ACS Macro Lett. 4 (2015) 947–951. doi:10.1021/acsmacrolett.5b00512.

[26] M. Yavari, T. Le, H. Lin, Physical aging of glassy perfluoropolymers in thin film composite membranes. Part I. Gas transport properties, J. Membr. Sci. 525 (2017) 387–398. doi:10.1016/j.memsci.2016.07.002.

[27] K. Nagai, T. Masuda, T. Nakagawa, B.D. Freeman, I. Pinnau, Poly[1-(trimethylsilyl)-1-propyne] and related polymers: synthesis, properties and functions, Prog. Polym. Sci. 26 (2001) 721–798. doi:10.1016/S0079-6700(01)00008-9.

[28] A. Fuoco, B. Satilmis, T. Uyar, M. Monteleone, E. Esposito, C. Muzzi, E. Tocci, M. Longo, M.P. De Santo, M. Lanč, K. Friess, O. Vopička, P. Izák, J.C. Jansen, Comparison of pure and mixed gas permeation of the highly fluorinated polymer of intrinsic microporosity PIM-2 under dry and humid conditions: Experiment and modelling, J. Membr. Sci. 594 (2020) 117460. doi:10.1016/j.memsci.2019.117460.

[29] A.X. Wu, J.A. Drayton, X. Ren, K. Mizrahi Rodriguez, A.F. Grosz, J.-W. Lee, Z.P. Smith, Non-equilibrium Lattice Fluid Modeling of Gas Sorption for Fluorinated Poly(ether imide)s, Macromolecules. 54 (2021) 6628–6638. doi:10.1021/acs.macromol.1c00950.

[30] J.C. Jansen, M. Lanč, Gas/Vapor Transport, in: E. Drioli, L. Giorno (Eds.), Encycl. Membr., Springer Berlin Heidelberg, Berlin, Heidelberg, 2016: pp. 859–871. doi:10.1007/978-3-662-44324-8_263.

[31] S.Y. Markova, T. Gries, V. V. Teplyakov, Poly(4-methyl-1-pentene) as a semicrystalline polymeric matrix for gas separating membranes, J. Membr. Sci. 598 (2020) 117754. doi:10.1016/J.MEMSCI.2019.117754.

[32] T.T. Moore, W.J. Koros, Gas sorption in polymers, molecular sieves, and mixed matrix membranes, J. Appl. Polym. Sci. 104 (2007) 4053–4059. doi:https://doi.org/10.1002/app.25653.

[33] L. Wang, J.-P. Corriou, C. Castel, E. Favre, Transport of Gases in Glassy Polymers under Transient Conditions: Limit-Behavior Investigations of Dual-Mode Sorption Theory, Ind. Eng. Chem. Res. 52 (2013) 1089–1101. doi:10.1021/ie2027102.

[34] J. Guzmán, L. Garrido, Determination of carbon dioxide transport coefficients in liquids and polymers by NMR spectroscopy, J. Phys. Chem. B. 116 (2012) 6050–6058. doi:10.1021/jp302037w.

[35] L. Garrido, C. García, M. López-González, B. Comesaña-Gándara, Á.E. Lozano, J. Guzmán, Determination of Gas Transport Coefficients of Mixed Gases in 6FDA-TMPDA Polyimide by NMR Spectroscopy, Macromolecules. 50 (2017) 3590–3597. doi:10.1021/acs.macromol.7b00384.

[36] M. Minelli, G.C. Sarti, Gas transport in glassy polymers: Prediction of diffusional time lag, Membranes (Basel). 8 (2018). doi:10.3390/membranes8010008.

749 [37] E. Tocci, D. Hofmann, D. Paul, N. Russo, E. Drioli, A molecular simulation study on gas diffusion in
750 a dense poly(ether–ether–ketone) membrane, Polymer (Guildf). 42 (2001) 521–533.
751 doi:10.1016/S0032-3861(00)00102-6.

752 [38] B. Kruczek, T. Matsuura, Limitations of a constant pressure-type testing system in determination of
753 gas transport properties of hydrophilic films, J. Membr. Sci. 177 (2000) 129–142. doi:10.1016/S0376-
754 7388(00)00454-3.

755 [39] K. Friess, J.C. Jansen, O. Vopička, A. Randová, V. Hynek, M. Šípek, L. Bartovská, P. Izák, M.
756 Dingemans, J. Dewulf, H. Van Langenhove, E. Drioli, Comparative study of sorption and permeation
757 techniques for the determination of heptane and toluene transport in polyethylene membranes, J.
758 Membr. Sci. 338 (2009) 161–174. doi:10.1016/j.memsci.2009.04.030.

759 [40] H.A. Daynes, The Process of Diffusion through a Rubber Membrane, Proc. R. Soc. A Math. Phys. Eng.
760 Sci. 97 (1920) 286–307. doi:10.1098/rspa.1920.0034.

761 [41] S.W. Rutherford, D.D. Do, Review of time lag permeation technique as a method for characterisation
762 of porous media and membranes, Adsorption. 3 (1997) 283–312. doi:10.1007/BF01653631.

763 [42] Y.-S. Lee, J.-H. Shim, J.-Y. Suh, A finite outlet volume correction to the time lag method: The case of
764 hydrogen permeation through V-alloy and Pd membranes, J. Membr. Sci. 585 (2019) 253–259.
765 doi:10.1016/j.memsci.2019.05.048.

766 [43] D. Bai, F. Asempour, B. Kruczek, Can the time-lag method be used for the characterization of liquid
767 permeation membranes?, Chem. Eng. Res. Des. 162 (2020) 228–237. doi:10.1016/j.cherd.2020.08.012.

768 [44] N. Al-Qasas, J. Thibault, B. Kruczek, A new characterization method of membranes with nonlinear
769 sorption isotherm systems based on continuous upstream and downstream time-lag measurements, J.
770 Membr. Sci. 542 (2017) 91–101. doi:10.1016/j.memsci.2017.07.039.

771 [45] B. KRUCZEK, H. FRISCH, R. CHAPANIAN, Analytical solution for the effective time lag of a
772 membrane in a permeate tube collector in which Knudsen flow regime exists, J. Membr. Sci. 256 (2005)
773 57–63. doi:10.1016/j.memsci.2005.02.006.

774 [46] S. Lashkari, B. Kruczek, H.L. Frisch, General solution for the time lag of a single-tank receiver in the
775 Knudsen flow regime and its implications for the receiver's configuration, J. Membr. Sci. 283 (2006)
776 88–101. doi:10.1016/j.memsci.2006.06.015.

777 [47] S. Lashkari, B. Kruczek, Effect of resistance to gas accumulation in multi-tank receivers on membrane
778 characterization by the time lag method. Analytical approach for optimization of the receiver, J. Membr.
779 Sci. 360 (2010) 442–453. doi:10.1016/j.memsci.2010.05.043.

780 [48] N. Al-Qasas, J. Thibault, B. Kruczek, The effect of the downstream pressure accumulation on the time-
781 lag accuracy for membranes with non-linear isotherms, J. Membr. Sci. 511 (2016) 119–129.
782 doi:10.1016/j.memsci.2016.03.047.

[49] G. Genduso, B.S. Ghanem, I. Pinnau, Experimental Mixed-Gas Permeability, Sorption and Diffusion of CO2-CH4 Mixtures in 6FDA-mPDA Polyimide Membrane: Unveiling the Effect of Competitive Sorption on Permeability Selectivity, Membranes (Basel). 9 (2019). doi:10.3390/membranes9010010.

[50] G. Genduso, Y. Wang, B.S. Ghanem, I. Pinnau, Permeation, sorption, and diffusion of CO2-CH4 mixtures in polymers of intrinsic microporosity: The effect of intrachain rigidity on plasticization resistance, J. Membr. Sci. 584 (2019) 100–109. doi:10.1016/j.memsci.2019.05.014.

[51] G. Genduso, E. Litwiller, X. Ma, S. Zampini, I. Pinnau, Mixed-gas sorption in polymers via a new barometric test system: sorption and diffusion of CO2-CH4 mixtures in polydimethylsiloxane (PDMS), J. Membr. Sci. 577 (2019) 195–204. doi:10.1016/J.MEMSCI.2019.01.046.

[52] E. Ricci, F.M. Benedetti, M.E. Dose, M.G. De Angelis, B.D. Freeman, D.R. Paul, Competitive sorption in CO2/CH4 separations: the case of HAB-6FDA polyimide and its TR derivative and a general analysis of its impact on the selectivity of glassy polymers at multicomponent conditions, J. Membr. Sci. 612 (2020) 118374. doi:https://doi.org/10.1016/j.memsci.2020.118374.

[53] J. Chen, L.S. Loo, K. Wang, A Novel Time Lag Method to Measure the Permeation of Vapor-Gas Mixtures, J. Membr. Sep. Technol. 1 (2012) 94–99. doi:10.6000/1929-6037.2012.01.02.3.

[54] H. Zhou, K.L. Goh, X. Feng, K. Wang, Measuring the permeabilities of binary gas mixtures with a novel time-lag technique, Can. J. Chem. Eng. n/a (n.d.). doi:https://doi.org/10.1002/cjce.24040.

[55] E. Ricci, E. Di Maio, M. Degli Esposti, L. Liu, G. Mensitieri, P. Fabbri, S.E. Kentish, M.G. De Angelis, Towards a systematic determination of multicomponent gas separation with membranes: the case of CO2/CH4 in cellulose acetates, J. Membr. Sci. 628 (2021) 119226. doi:10.1016/j.memsci.2021.119226.

[56] D. Hofmann, L. Fritz, J. Ulbrich, D. Paul, Molecular simulation of small molecule diffusion and solution in dense amorphous polysiloxanes and polyimides, Comput. Theor. Polym. Sci. 10 (2000) 419–436.

[57] T. Schäfer, J. Vital, J.G. Crespo, Coupled pervaporation/mass spectrometry for investigating membrane mass transport phenomena, J. Membr. Sci. 241 (2004) 197–205. doi:10.1016/j.memsci.2004.05.014.

[58] C. Brazinha, A.P. Fonseca, O.M.N.D. Teodoro, J.G. Crespo, On-line and real-time monitoring of organophilic pervaporation by mass spectrometry, J. Membr. Sci. 347 (2010) 83–92. doi:10.1016/j.memsci.2009.10.009.

[59] P. Tremblay, M.M. Savard, J. Vermette, R. Paquin, Gas permeability, diffusivity and solubility of nitrogen, helium, methane, carbon dioxide and formaldehyde in dense polymeric membranes using a new on-line permeation apparatus, J. Membr. Sci. 282 (2006) 245–256. doi:10.1016/j.memsci.2006.05.030.

[60] S.C. Fraga, M.A. Azevedo, I.M. Coelhoso, C. Brazinha, J.G. Crespo, Steady-state and transient

transport studies of gas permeation through dense membranes using on-line mass spectrometry, Sep. Purif. Technol. 197 (2018) 18–26. doi:10.1016/j.seppur.2017.12.026.

[61] S.C. Fraga, L. Trabucho, C. Brazinha, J.G. Crespo, Characterisation and modelling of transient transport through dense membranes using on-line mass spectrometry, J. Membr. Sci. 479 (2015) 213–222. doi:10.1016/j.memsci.2014.12.016.

[62] K. Pilnacek, J.C. Jansen, P. Bernardo, G. Clarizia, F. Bazzarelli, F. Tasselli, Determination of Mixed Gas Permeability of High Free Volume Polymers Using Direct Mass Spectrometric Analysis of the Gas Compositions, Procedia Eng. 44 (2012) 1027–1029. doi:10.1016/j.proeng.2012.08.664.

[63] S.C. Fraga, M. Monteleone, M. Lanč, E. Esposito, A. Fuoco, L. Giorno, K. Pilnáček, K. Friess, M. Carta, N.B. McKeown, P. Izák, Z. Petrusová, J.G. Crespo, C. Brazinha, J.C. Jansen, A novel time lag method for the analysis of mixed gas diffusion in polymeric membranes by on-line mass spectrometry: Method development and validation, J. Membr. Sci. 561 (2018) 39–58. doi:10.1016/j.memsci.2018.04.029.

[64] M. Monteleone, E. Esposito, A. Fuoco, M. Lanč, K. Pilnáček, K. Friess, C. Bezzu, M. Carta, N. McKeown, J.C. Jansen, A Novel Time Lag Method for the Analysis of Mixed Gas Diffusion in Polymeric Membranes by On-Line Mass Spectrometry: Pressure Dependence of Transport Parameters, Membranes (Basel). 8 (2018) 73. doi:10.3390/membranes8030073.

[65] E. V Evans, C.N. Kenney, Gaseous dispersion in laminar flow through a circular tube, Proc. R. Soc. London. Ser. A. Math. Phys. Sci. 284 (1965) 540–550. doi:10.1098/rspa.1965.0079.

[66] G.I. Taylor, Dispersion of soluble matter in solvent flowing slowly through a tube, Proc. R. Soc. London. Ser. A. Math. Phys. Sci. 219 (1953) 186–203. doi:10.1098/rspa.1953.0139.

[67] I.N. Beckman, M.G. Shalygin, V. V. Teplyakov, Particularities of Membrane Gas Separation Under Unsteady State Conditions, in: J. Markoš (Ed.), Mass Transf. Chem. Eng. Process., InTech, Rijeka, 2011: pp. 205–232. doi:10.5772/24112.

[68] I.N. Beckman, D.A. Syrtsova, M.G. Shalygin, P. Kandasamy, V.V. Teplyakov, Transmembrane gas transfer: Mathematics of diffusion and experimental practice, J. Membr. Sci. 601 (2020) 117737. doi:10.1016/J.MEMSCI.2019.117737.

[69] A. Fuoco, M. Monteleone, E. Esposito, R. Bruno, J. Ferrando-Soria, E. Pardo, D. Armentano, J.C. Jansen, Gas Transport in Mixed Matrix Membranes: Two Methods for Time Lag Determination, Computation. 8 (2020) 28. doi:10.3390/computation8020028.

[70] C.R. Mason, L. Maynard-Atem, K.W.J. Heard, B. Satilmis, P.M. Budd, K. Friess, M. Lanč, P. Bernardo, G. Clarizia, J.C. Jansen, Enhancement of CO2 Affinity in a Polymer of Intrinsic Microporosity by Amine Modification, Macromolecules. 47 (2014) 1021–1029. doi:10.1021/ma401869p.

851 [71] B. Satilmis, M. Lanč, A. Fuoco, C. Rizzuto, E. Tocci, P. Bernardo, G. Clarizia, E. Esposito, M.
852 Monteleone, M. Dendisová, K. Friess, P.M. Budd, J.C. Jansen, Temperature and pressure dependence
853 of gas permeation in amine-modified PIM-1, J. Membr. Sci. 555 (2018) 483–496.
854 doi:10.1016/j.memsci.2018.03.039.

855 [72] R. Scheichl, M.H. Klopffer, Z. Benjelloun-Dabaghi, B. Flaconnèche, Permeation of gases in polymers:
856 Parameter identification and nonlinear regression analysis, J. Membr. Sci. 254 (2005) 275–293.
857 doi:10.1016/j.memsci.2005.01.019.

858 [73] O. Vopička, K. Friess, V. Hynek, P. Sysel, M. Zgažar, M. Šípek, K. Pilnáček, M. Lanč, J.C. Jansen,
859 C.R. Mason, P.M. Budd, Equilibrium and transient sorption of vapours and gases in the polymer of
860 intrinsic microporosity PIM-1, J. Membr. Sci. 434 (2013) 148–160.
861 doi:10.1016/j.memsci.2013.01.040.

862 [74] O. Vopička, M. Lanč, K. Friess, Phenomenology of vapour sorption in polymers of intrinsic
863 microporosity PIM-1 and PIM-EA-TB: envelopment of sorption isotherms, Curr. Opin. Chem. Eng. 35
864 (2022) 100786. doi:10.1016/j.coche.2021.100786.

865 [75] A. Fuoco, B. Comesaña-Gándara, M. Longo, E. Esposito, M. Monteleone, I. Rose, C.G. Bezzu, M.
866 Carta, N.B. McKeown, J.C. Jansen, Temperature Dependence of Gas Permeation and Diffusion in
867 Triptycene-Based Ultrapermeable Polymers of Intrinsic Microporosity, ACS Appl. Mater. Interfaces.
868 10 (2018) 36475–36482. doi:10.1021/acsami.8b13634.

869 [76] S.M. Jordan, W.J. Koros, G.K. Fleming, The effects of CO2 exposure on pure and mixed gas
870 permeation behavior: comparison of glassy polycarbonate and silicone rubber, J. Membr. Sci. 30 (1987)
871 191–212. doi:https://doi.org/10.1016/S0376-7388(00)81351-4.

872 [77] D.R. Paul, W.J. Koros, Effect of partially immobilizing sorption on permeability and the diffusion time
873 lag, J. Polym. Sci. Polym. Phys. Ed. 14 (1976) 675–685. doi:10.1002/pol.1976.180140409.

874 [78] S.M. Jordan, W.J. Koros, Permeability of pure and mixed gases in silicone rubber at elevated pressures,
875 J. Polym. Sci. Part B Polym. Phys. 28 (1990) 795–809.
876 doi:https://doi.org/10.1002/polb.1990.090280602.

877 [79] E. Favre, N. Morliere, D. Roizard, Experimental evidence and implications of an imperfect upstream
878 pressure step for the time-lag technique, J. Membr. Sci. 207 (2002) 59–72. doi:10.1016/S0376-
879 7388(02)00039-X.

880 [80] P. Stanovsky, M. Karaszova, Z. Petrusova, M. Monteleone, J.C. Jansen, B. Comesaña-Gándara, N.B.
881 McKeown, P. Izak, Upgrading of raw biogas using membranes based on the ultrapermeable polymer
882 of intrinsic microporosity PIM-TMN-Trip, J. Membr. Sci. 618 (2021) 118694.
883 doi:10.1016/j.memsci.2020.118694.

884 [81] C.G. Bezzu, A. Fuoco, E. Esposito, M. Monteleone, M. Longo, J.C. Jansen, G.S. Nichol, N.B.

McKeown, Ultrapermeable Polymers of Intrinsic Microporosity Containing Spirocyclic Units with Fused Triptycenes, Adv. Funct. Mater. 31 (2021) 2104474. doi:10.1002/adfm.202104474.

[82] J. Crank, G.S. Park, Diffusion in Polymers, Academic Press, London & New York, 1968. https://books.google.it/books?id=TJkpcAAACAAJ.

[83] J. Crank, The mathematics of diffusion, 2nd ed., Clarendon Press, Oxford, 1975. https://books.google.it/books/about/The_mathematics_of_diffusion.html?id=7QjwAAAAMAAJ&redir_esc=y.

[84] J.C. Jansen, K. Friess, E. Drioli, Organic vapour transport in glassy perfluoropolymer membranes: A simple semi-quantitative approach to analyze clustering phenomena by time lag measurements, J. Membr. Sci. 367 (2011) 141–151. doi:10.1016/j.memsci.2010.10.063.

[85] L.B. Loeb, The Kinetic Theory of Gases, Dover Publications, Inc., New York, 1961.

[86] V. Teplyakov, P. Meares, Correlation aspects of the selective gas permeabilities of polymeric materials and membranes, Gas Sep. Purif. 4 (1990) 66–74. doi:10.1016/0950-4214(90)80030-O.